Title

Detection of protein–protein interactions at the septin collar in Saccharomyces cerevisiae using a tripartite split-GFP system

Journal

Molecular Biology of the Cell, 27(17)

ISSN

1059-1524

Authors

Finnigan, Gregory C
Duvalyan, Angela
Liao, Elizabeth N
et al.

Publication Date

2016-09-01

DOI

10.1091/mbc.e16-05-0337

Peer reviewed

Detection of protein-protein interactions at the septin collar in *Saccharomyces cerevisiae* using a tripartite split-GFP system

Gregory C. Finnigan,[†] Angela Duvalyan, Elizabeth N. Liao, Aspram Sargsyan and Jeremy Thorner*

Division of Biochemistry, Biophysics and Structural Biology,

Department of Molecular and Cell Biology,

University of California, Berkeley, CA 94720-3202 USA

Running title: Protein-septin association assessed by GFP reconstitution

[†]Current address: Dept. of Biochemistry and Molecular Biophysics, Kansas State University, Manhattan, KS 66506

*Correspondence to: Jeremy Thorner; Tel. (510) 642-2558; FAX (510) 642-6420; E-mail: jthorner@berkeley.edu

Abbreviations: APC, anaphase-promoting complex; β10, the 10th *beta* strand of the evolved eGFP variant of the tripartite split-GFP system; β11, the 11th *beta* strand of the evolved eGFP variant of the tripartite split-GFP system; BiFC, bimolecular fluorescence complementation; CaaX, prenylation site consensus motif (where C is the prenylated cysteine, a is any aliphatic residue, and the residue at X dictates farnesylation or geranylgeranylation); CTE, C-terminal extension; D-box, destruction box (motif for recognition of a substrate via mutual engagement by the Cdc10 and Cdc20 subunits of the APC); eGFP, enhanced green fluorescent protein; EM, electron microscope; 5-FOA, 5-fluoro-orotic acid; FRET, Foerster resonance energy transfer; GFPβ1-9, the stable *beta* barrel of the evolved eGFP variant of the tripartite split-GFP system; KA1, kinase associated-1 domain; KEN box, motif for substrate recognition by either the Cdc20 or Cdh1 subunits of the APC; mCh, monomeric red fluorescent protein mCherry; NLS, nuclear localization signal; PCA, protein-fragment complementation; PM, plasma membrane; PtdIns4,5P_2, phosphatidylinositol-4,5-*bis*-phosphate; PtdSer, phosphatidylserine; YFP, yellow variant of eGFP.

ABSTRACT

A variety of methods have been devised that can provide a read-out of the physical interaction between two biomolecules. A recently described tripartite split-GFP system [Cabantous S *et al.* (2013) *Sci. Rep*. **3**: 2854.1-2854.9] has the potential to report by direct visualization via a fluorescence signal the intimate association of minimally-tagged proteins expressed at their endogenous level in their native cellular milieu and can capture transient or weak interactions. Here we document the utility of this tripartite split-GFP system to assess in living cells protein-protein interactions in a dynamic cytoskeletal structure, the septin collar at the yeast bud neck. We show, first, that for septin-septin interactions this method yields a robust signal whose strength reflects the known spacing between the subunits in septin filaments and thus serves as a "molecular ruler." Second, the method yields little or no spurious signal even with highly abundant cytosolic proteins readily accessible to the bud neck (including molecular chaperone Hsp82 and glycolytic enzyme Pgk1). Third, using two proteins (Bni5 and Hsl1) that have been shown by other means to bind directly to septins at the bud neck *in vivo*, we validate that the tripartite split-GFP method yields the same conclusions and further insights about specificity. Finally, we demonstrate the capacity of this approach to uncover additional new information by examining whether three other proteins reported to localize to the bud neck (Nis1, Bud4 and Hof1) are able to interact physically with any of the subunits in the septin collar and, if so, with which ones.

INTRODUCTION

In eukaryotic cells, structures built with septins, a conserved family of GTP-binding proteins, serve a number of functions, including associating with and deforming the plasma membrane (PM) (Bridges and Gladfelter, 2015), erecting a barrier to restrict diffusion and establish subcellular compartments (Saarikangas and Barral, 2011), and providing a three-dimensional scaffold to localize the action of enzymes and other proteins spatially and temporally (McMurray and Thorner, 2009; Oh and Bi, 2011). The first septin-based structure was visualized by EM in budding yeast (*Saccharomyces cerevisiae*) as an hour-glass shaped collar of circumferential bands located at the bud neck between a mother and daughter cell undergoing mitosis (Byers and Goetsch, 1976). Genetic and cytological analysis demonstrated that products of four mitotically expressed genes (*CDC3*, *CDC10*, *CDC11* and *CDC12*) (Hartwell, 1971; Hartwell et al., 1974) are necessary to form this structure, are integral components of this structure (Cid et al., 1998; Haarer and Pringle, 1987), and are required for the execution of cytokinesis and cell septation (Wloka and Bi, 2012). A fifth mitotically expressed septin gene (*SHS1*) was identified by other means (Carroll et al., 1998; Mino et al., 1998) and appears to be a recently evolved non-essential paralog of *CDC11* (Iwase et al., 2007; Garcia et al., 2011).

The products of these yeast septin genes assemble into two classes of linear hetero-octamers (Cdc11-Cdc12-Cdc3-Cdc10-Cdc10-Cdc3-Cdc12-Cdc11 and Shs1-Cdc12-Cdc3-Cdc10-Cdc10-Cdc3-Cdc12-Shs1). These subunit arrangements were determined by EM examination of recombinant septin complexes containing tagged subunits (Bertin et al., 2008; Garcia et al., 2011) and amply confirmed *in vivo* by numerous genetic experiments (McMurray et al., 2011; Finnigan et al., 2015b). In humans, the basic building blocks of septin structures are also hetero-octamers that have the capacity to self-assemble into higher-order ensembles (Hall and Russell, 2012; Mostowy and Cossart, 2012; Fung et al., 2014).

In vitro, Cdc11-capped hetero-octamers polymerize end-to-end into long straight filaments that pair in register via cross-filament interactions mediated by the C-terminal extensions (CTEs)

of both Cdc3 and Cdc12 (Versele et al., 2004; Bertin et al., 2008). Shs1-capped hetero-octamers, by contrast, bundle laterally to form arcs, spirals and rings (Garcia et al., 2011). Together, these two types of hetero-octamers, in conjunction with the collective actions of scores of other bud neck-localized proteins (Gladfelter et al., 2001; McMurray and Thorner, 2009), are responsible for the state of supramolecular assembly and function of septin structures during progression through the cell cycle (Bi and Park, 2012). In early G1, septins form a small patch at the incipient bud site that resolves into a ring and then expands, as the bud emerges, into the hourglass-shaped collar, which, at the onset of cytokinesis, is split (or collapses, like two accordions) into two, tighter gasket-like bands that trap between them proteins that execute cell division.

Yeast proteins that localize at various times and to varying degrees in the near vicinity of septin structures include factors that participate in diverse processes— from cell polarity and vesicular transport, to cell cycle control, actomyosin contractile ring assembly, and cell wall deposition. Similarly, septin-based structures and their associated proteins appear responsible for a range of specialized functions in mammalian cells, including the annulus in spermatozoa (Toure et al., 2011) and assemblies found at the base of the primary cilium (Malicki and Avidor-Reiss, 2014) and in the neck of the dendritic spines on neurons (Ewers et al., 2014).

For the majority of the proteins that reportedly co-localize with the septin collar at the bud neck, it remains unclear whether their localization is septin-dependent and, if so, whether they are recruited because they bind directly to a septin(s). Moreover, for those factors known to be direct interaction partners, it is not known whether they recognize a structural feature unique to a given septin or one generated only upon higher-order septin assembly.

A variety of methods have been developed to assess the physical encounter of two molecules in the cell, from FRET (Padilla-Parra and Tramier, 2012) to a number of protein-fragment complementation assays (PCA) (Remy and Michnick, 2015) with readouts as diverse as drug resistance, enzyme activity, colorimetric changes, or a fluorescent signal. Among the

PCA approaches, bimolecular fluorescence complementation (BiFC) has gained rather wide acceptance (Magliery et al., 2005; Kerppola, 2009; Ohashi and Mizuno, 2014; Miller et al., 2015) because it can detect even weak or transient interactions for the reason that once two associating proteins bring the two halves of the fluorescent reporter protein together, reconstitution of the reporter stabilizes the complex. In addition, BiFC does not require cell fixation, cell lysis, or any special treatment with dyes or other reagents. However, a limitation of BiFC is that the proteins tested for interaction need to be fused to the halves of the fluorescent reporter (typically, YFP), which are rather bulky tags that may perturb the interaction under study or may be fused to each partner in inappropriate orientations that prevent reconstitution.

Therefore, to commence a systematic examination of whether any given bud neck-localized protein intimately associates with any subunit(s) of the septin collar, we chose to implement a fluorescence-based tripartite split-GFP methodology (Cabantous et al., 2013) for assessing protein-protein interaction because, in this system, the tags appended to the test proteins are of minimal size and can be attached by flexible tethers. Binding of a protein bearing at its N terminus the β10 strand (20 residues) of an evolved eGFP variant to a protein bearing at its C terminus the β11 strand (21 residues) of this variant permits capture of the otherwise non-fluorescent GFPβ1-9 barrel (200 residues) of the same variant, allowing for reconstitution of eGFP structure and fluorophore formation, yielding a stable fluorescence readout.

As described here, we were able to utilize this approach *in vivo* (i) to robustly detect subunit-subunit interactions within the septin hetero-octamer, (ii) to document that illegimate interactions with non-physiological partners are minimal-to-undetectable; (iii) to use two septin-associated proteins with known septin-binding capacity to validate that this method authentically detects direct physical interaction; and, (iv) to assess the septin-binding selectivity of three bud neck-localized proteins whose septin association *per se* has not been positively characterized previously. We also demonstrate that variation of the fluorescent signal with tether length provides a novel molecular ruler for measuring distances at the nanometer scale.

RESULTS

Rationale for utilization of the tripartite split-GFP protein-protein interaction system

Various experimental strategies have been applied to determine the molecular organization of the septin superstructure that demarcates the division site in a budding yeast cell. Recombinant protein expression, *in vitro* reconstitution and ultrastructural analysis by EM revealed the linear, apolar hetero-octameric arrangement of the septin subunits in mitotic cells (Versele and Thorner, 2004; Farkasovsky et al., 2005; Bertin et al., 2008; Garcia et al., 2011). Genetic analyses have confirmed subunit order *in vivo* and helped to delineate the contributions of individual subunits and their domains to the physiological functions of septins (McMurray et al., 2011; Finnigan et al., 2015a; Finnigan et al., 2015b). Genome-wide cytological studies, including indirect immunofluorescence of epitope-tagged proteins (Kumar et al., 2002) and direct visualization of GFP-tagged proteins (Huh et al., 2003), has provided a partial catalog of proteins that localize to the bud neck. Other tactics for detecting protein-protein interaction have also been exploited to discern what other proteins associate with septins, including the two-hybrid screen (Drees et al., 2001), FRET analysis (Booth et al., 2015), a variant of the split-ubiquitin reconstitution system (dubbed SPLIFF) (Dunkler et al., 2015), and affinity purification followed by mass spectrometry (Renz et al., 2016). Every approach has, however, its own inherent disadvantages and limitations in terms of sensitivity of detection, throughput, and/or application to live cells.

To initiate a systematic study to assess whether any given cellular protein is able to bind directly to a septin at the bud neck, we felt that a newly devised tripartite split-GFP system (Cabantous et al., 2013) had many advantages for assessing intimate physical contact between two proteins. First, this method involves the attachment of unstructured tags of minimal size to the target proteins of interest [N-terminal β10 (20 residues); C-terminal β11 (21 residues)] (Fig, S1). Unlike attachment of the much bulkier reporters required for other methods, this feature greatly reduces the likelihood that presence of the tag itself will compromise the structure or

function of the target protein, or interfere sterically with the binding interface between the two target proteins, or occlude a localization signal responsible for delivery to the proper cellular compartment *in situ*. Second, the tags can be anchored to the target proteins via flexible tethers (linker sequences) of variable length (Fig. S1). This property obviates the need for the tags to be installed in any particular orientation and, as we demonstrate, provides a means by which this system can be used to assess the separation distance between two target proteins on a biologically-relevant length scale. Third, the readout in this system involves capture by the tags of a GFPβ1-9 barrel expressed as a free protein, an encounter that can only occur at a detectable level if the β10 and β11 tags are held in close proximity via association of the two target proteins. This three-way association reconstitutes eGFP, allows for formation of its fluorophore, and thereby further stabilizes interaction between the two target proteins. Thus, this system can detect even weak or transient protein-protein interactions and yields a convenient fluorescent output for the positives.

Implementation of the tripartite split-GFP system for detecting septin interactions *in vivo*

As our initial test of the efficacy of the tripartite split-GFP method to detect authentic protein-protein interactions in live yeast cells, and given that the order of the subunits in septin complexes is well-defined and invariant, we examined whether this method would accurately report the known arrangement of the septin subunits. We utilized the following experimental design (Fig. 1A). First, in *MAT*α cells, a protein of interest was tagged at its N terminus with β10 and expressed from its endogenous promoter at its normal chromosomal locus (Table 1). To mark the bud neck, these same cells also expressed either Cdc10-mCh (or Cdc11-mCh) from its endogenous promoter at its normal chromosomal locus. Second, in *MAT***a** cells, another protein of interest was tagged at its C terminus with β11 and expressed from its endogenous promoter at its normal chromosomal locus (Table 1). These same cells carried a *CEN* plasmid that expresses the GFPβ1-9 barrel under control of the inducible *GAL1/10* promoter (Table 2), allowing for control of both the level and timing of its expression. Therefore, to assess the

interaction between any two proteins (*e.g.*, two septin subunits), the appropriate *MAT***a** and *MAT*α haploids were mated, the resulting diploid grown on galactose-containing medium (thereby providing all three components of the tripartite split-GFP system in the same cell), and then examined under the fluorescence microscope.

As our first proof of principle, we asked whether we could readily detect the interaction between the two Cdc10 monomers that are juxtaposed at the center of the hetero-octamer (Fig. S1A). Indeed, in diploids co-expressing β10-Cdc10, Cdc10-β11 and GFPβ1-9 a very bright green fluorescent signal was generated in the vast majority (>90%) of the cells that was confined to and congruent with the septin collar at the bud neck, which was marked with Cdc11-mCh (Fig. 1B). Importantly, when examined for the same exposure time, in diploids produced from mating otherwise isogenic strains lacking any one of the tripartite split-GFP components, there was virtually no detectable signal above the background of the intrinsic fluorescence of a yeast cell measured using the cut-off filters we employed (Fig. 1B). Quantification of the average pixel intensity at the bud neck for the cells expressing β10-Cdc10, Cdc10-β11 and GFPβ1-9 indicated that the fluorescent signal was more than 20-fold brighter than any of the negative controls (Fig, 1C). Using this same readout, we found that either of two different versions of the GFPβ1-9 barrel (Cabantous et al., 2013) that differ by 4 residues at their C-terminal end *(i.e.*, just downstream of β9) yielded equally robust fluorescence signals (Fig. S2).

Our next concern was to eliminate the possibility that the tripartite split-GFP system might erroneously report adventitious and physiologically irrelevant interactions. Therefore, we tested whether any of five gene products that are reportedly among the most abundant cytosolic proteins in *S. cerevisiae* (some estimates as high as 300,000-500,000 molecules per cell; Table S4) could produce a significant degree of fluorescence by this method. Each of these candidates (Cdc19, Gpp1, Hsp82, Pgk1 and Tpi1) when expressed as a C-terminally GFP-tagged derivative from its endogenous promoter at its native chromosomal locus exhibited a very prominent cytosolic distribution (Fig. 1D, *left*) and, thus, should be readily accessible to the

septin collar at the bud neck. Although none of these five test proteins has any interaction of any kind with any septin subunit recorded in the literature, with the single exception of a purported 2-hybrid interaction between Cdc12 and Hsp82 (Millson et al., 2005), we reasoned that, if the tripartite split-GFP system were prone to false positives generated by random encounters, that such would be revealed with such abundantly expressed proteins. To maximally challenge the tripartite split-GFP system and give it every opportunity to produce a spurious readout, we appended the β11 tag to the C-terminal end of each of the five test proteins via a flexible 33-residue linker and we crossed strains producing them against a strain expressing N-terminally β10-tagged Cdc3, which, of all the mitotic septins, is the subunit with the longest N-terminal extension (Fig. S1B). Very reassuringly, with β10-Cdc3 (Fig. 1D) and every other β10-tagged septin (Fig. 1E), we found that the majority of the cells expressing Hsp82-β11 and Gpp1-β11 exhibited virtually no detectable signal at the bud neck above the intrinsic fluorescence of yeast cells and that the cells expressing Pgk1-β11, Cdc19-β11, and Tpi1-β11 displayed very weak fluorescent signals that were never more than 2-3 fold above the intrinsic background fluorescence.

Tripartite split-GFP readout accurately reflects distant constraints in septin complexes

Having found a robust readout for the interaction between the two tagged Cdc10 monomers (β10-Cdc10 and Cdc10-β11) that constitute the central core of the septin hetero-octamer, we reasoned that a further test of this system to report authentic protein-protein interactions would be to examine whether the readout obtained would accurately represent the known distance relationships between Cdc10 and the other subunits in the septin hetero-octamer. For this reason, and using the same overall strategy (Fig. 1A), we generated diploids in which we assessed the ability of Cdc10-β11 to interact with N-terminally β10-tagged versions of each of the other septins (Fig. 2). Gratifyingly, when the β10 or β11 tags were appended to a septin using linkers of minimal length, we found that Cdc10-β11 strongly interacted with only its immediately neighboring subunits, either β10-Cdc10 or β10-Cdc3, respectively, in the vast

majority of the cells (80-90%) (Figs. 2A and 2B).

We next explored the possibility that extending the length of the linker (Fig. S1A) might allow for detection of association with a stably held, but somewhat more distantly located, interaction partner. For this purpose. we varied the length of the linker in Cdc10-β11 from 0 to 10, 20 and 33 residues and also increased the length of the linker in the N-terminally β10-tagged versions of each of the other septins from 5 to 18 residues, and generated the respective diploids. For the expected interactions (Cdc10-Cdc10 and Cdc10-Cdc3), we found that increasing the tether length had a negligible effect on the percentage of the cell population exhibiting an obvious fluorescent signal at the bud neck (Fig. 2B), but did progressively enhance the strength of that fluorescent signal (Fig. 2C). Moreover, and strikingly, when the tether length was increased, interaction of Cdc10-β11 with β11-Cdc12 became detectable, with both the fraction of the cells displaying a detectable signal and the pixel intensity of the signal increasing with increasing linker length (Fig. 2C and Fig. S3). Nonetheless, on both an absolute and relative scale, the output from the nearest-neighbor Cdc10-Cdc10 and Cdc10-Cdc3 interactions was much more robust (at least an order of magnitude brighter) than that from the longer range Cdc10-Cdc12 interaction regardless of linker length (Fig. 2C). Moreover, regardless of linker length, no interaction between the centrally disposed Cdc10 subunit and either of the alternative terminal subunits (Cdc11 and Shs1) was detectable. Thus, our findings indicate, first, that the tripartite split-GFP system accurately reflects the spatial relationships among the subunits of the septin hetero-octamer. Second, because were able to detect, albeit weakly, interaction between Cdc10-β11 with β11-Cdc12 by extending the linker length between each tag and its cognate protein (which we estimate to be ~10 nm apart), systematic variation of the length of these tethers provides, in principle, a "molecular ruler" to estimate the maximum distance or limit of detection in this *in vivo* protein-protein interaction system, although such spacing constraints may vary significantly depending on the size and flexibility of the native N and C termini in the two proteins being tested, as is the case for the septins (Fig. S1B). Moreover, for septin-septin

interactions, especially at long tether lengths, the possibility of cross-filament interactions needs to be considered.

To further explore the inherent effects of the variability among the septins in the lengths of their native N and C termini (Fig. S1B) on the readout generated by the tripartite split-GFP system, we generated constructs in which the N-terminal β10 tag was appended to each septin by a minimal tether (5 residues) and the β11 tag was appended to the C terminus of each septin without any spacer at all. Similar to Cdc10-β11 tested against N-terminally β10-tagged versions of the other septins (Fig. 2), β10-Cdc10 tested against C-terminal β11-tagged versions of the other septins, yielded a robust signal with Cdc10-β11, as expected. However, compared to the nearest neighbor interaction assessed by testing Cdc10-β11 against β10-Cdc3, β10-Cdc10 tested against Cdc3-β11 yielded a detectable, but much weaker, signal (Fig. 3A and 3E, *left*). Also, β10-Cdc10 tested against Cdc12-β11 yielded a weak, but readily detectable, signal, quite akin to what we observed between Cdc10-β11 and β10-Cdc12 when we increased their linker lengths. Similarly, β10-Cdc3 tested against C-terminal β11-tagged versions of the other septins yielded the strongest output with the immediately juxtaposed subunits in the hetero-octamer (Cdc10-β11 and Cdc12-β11); however, β10-Cdc3 was also able to generate significant fluorescent signals with itself (Cdc3-β11) and the most distal subunits (Cdc11-β11 and Shs1-β11) (Fig. 3B and 3E, *middle left*). We presume this increased "promiscuity" is due to the fact that, unlike the other four septins, Cdc3 has a prominent (107 residues) N-terminal extension (Fig. S1B). By contrast, β10-Cdc12 generated its highest fluorescent signals only with its immediately juxtaposed subunits (Cdc3-β11, Cdc11-β11 and Shs1-β11), whereas its interaction with the most distant subunit (Cdc10-β11) was barely above background (Fig. 3C and 3E, *middle right*). The fact that Shs1 has the longest CTE of any septin (Fig. S1B) may explain why the combination of β10-Cdc12 and Shs1-β11 yielded the topmost signal. For β10-Cdc11, readily detectable signals were observed with its immediately adjacent subunit Cdc12-β11 and with the subunits (Cdc11-β11 and Shs1-β11) with which it forms, respectively, both homotypic and

heterotypic junctions when hetero-octamers polymerize into filaments (Booth et al., 2015; Finnigan et al., 2015b); however, β10-Cdc11 also displayed equivalent interaction with Cdc3-β11, presumably due to the length of the CTE present in Cdc3 (Fig. 3C and 3E, *middle right*). Finally, β10-Shs1 also displayed a detectable signal with its immediately adjacent subunit (Cdc12-β11), but significantly more robust signals with itself and with the subunit (Cdc11-β11) with which it forms a heterotypic junction in polymerized filaments (Fig. S4). As observed for β10-Cdc11, β10-Shs1 also displayed interaction with Cdc3-β11, again presumably due to the length of the CTE present in Cdc3. Thus, in summary, although not obviating the ability to detect both authentic and nearby interaction partners, the positions of the tags clearly do affect their accessibility and, hence, the efficiency of their encounter and ability to capture the GFPβ1-9 barrel and produce a readout.

In this same regard, one potential drawback to placing the β10 tag on the N terminus of either Cdc11 or Shs1 is that, even with the 5-residue spacer used, these two septins natively lack a significant extension upstream of the polybasic tract present in their α0 helix (Fig. S1B). These basic residues are thought to mediate interaction with PtdIns4,5P_2 on the inner leaflet of the PM (Bertin et al., 2010) and are required for the full *in vivo* function of these septins (Finnigan et al., 2015b). Thus, access to a tag placed at the N terminus of either of these two septins may be limited, resulting in a weaker signal in this assay format.

Validating the ability of the tripartite split-GFP method to detect septin-binding proteins

To verify that the tripartite split-GFP method can also faithfully report direct interaction of other cellular proteins with septins at the bud neck, we first examined Bni5 (448 residues). Bni5 is recruited to the bud neck prior to assembly of the actomyosin ring and is ejected from the bud neck by the time the septin collar has split (Fang et al., 2010; Schneider et al., 2013), as we also observed (Fig. 4A). There is ample evidence from two-hybrid (Lee et al., 2002) and mutational analysis (Finnigan et al., 2015a) *in vivo* and FRET (Booth et al., 2015) and EM analysis (Patasi et al., 2015) *in vitro* that Bni5 physically associates with septins Cdc11 and Shs1. We examined,

first, the interaction of C-terminally tagged Bni5-β11 with N-terminally β10-tagged versions of the five mitotic septins. Despite the fact that, for the reasons mentioned above, the N-termini of Cdc11 and Shs1 are liable to be less accessible than for the other three septins, Bni5-β11 exhibited a readily detectable interaction with β10-Cdc11 and β10-Shs1, and displayed no detectable interaction with β10-Cdc3, β10-Cdc10 or β10-Cdc12 (Fig. 4B and 4C). These results are in agreement with the published subunit selectivity of Bni5 and with the fact that deletion analysis showed that only the C-terminal third of Bni5 is required for its function (Finnigan et al., 2015a). However, structure prediction indicates that Bni5 is likely a highly elongated protein comprising a long bundle of nearly all α-helical segments with significant separation between its N and C termini (Finnigan et al., 2015a). Therefore, we also examined the interaction of N-terminally tagged β10-Bni5 with C-terminally β11-tagged versions of the five mitotic septins. Although the strongest interactions observed were once again between β10-Bni5 and Cdc11-β11 and Shs1-β11, nearly equivalent outputs were observed with the next nearest subunit (Cdc12-β11) and even the more distantly positioned subunits (Cdc3-β11 and Cdc10-β11) (Fig. 4D and 4E). Taken together, these data support the conclusion that the C-terminal end of Bni5 is anchored to Cdc11 and Shs1, whereas the N-terminal end of this highly elongated protein is more flexible and can sweep out a much larger conformational space. By contrast, we detected no interaction between β10-Bni5 and Bni5-β11, suggesting that this protein either does not readily self-associate or forms oligomers that are obligatorily in the parallel orientation.

Another protein for which there is now incontrovertible evidence that it contains a domain by which it physically associates with septins is the large (1518 residues) protein kinase Hsl1 (Finnigan et al., 2016). Hsl1 is recruited to the bud neck at the onset of bud emergence (Shulewitz et al., 1999) (Fig. 5A, *top*), but then is eliminated prior to cytokinesis because it is targeted for proteasome-mediated destruction by the cell cycle-regulated protein-ubiquitin ligase (E3) known as the anaphase-promoting complex (APC) (Burton and Solomon, 2000). Like the full-length enzyme (Fig. 5A, *top*), a fragment of Hsl1 (611-950) containing its septin-binding

domain is localized exclusively at the bud neck (especially when it is confined to the cytosol by mutational removal of a cryptic NLS) (Fig. 5A, *middle*), as documented recently (Finnigan et al., 2016). Moreover, as observed for full-length Hsl1 (Finnigan et al., 2016), presence of the C-terminal PtdSer-binding KA1 domain of Hsl1 is able to override the effect of the NLS and greatly enhance the ability of the 611-950 fragment to engage the septins at the bud neck (Fig. 5A, *middle*). Finally, because both the D box and KEN box by which the APC recognizes Hsl1 (Burton and Solomon, 2001) also reside within the 611-950 fragment, their mutational elimination increases the steady-state level of this fragment (Finnigan et al., 2016). Although the septin-binding region of Hsl1 has been delineated, the subunit specificity of Hsl1 binding to the septin collar, if any, has not yet been determined.

For the preceding reasons, we tested first whether we could detect association of N-terminally β10-tagged full-length Hsl1 with C-terminally β11-tagged versions of the five mitotic septins. This arrangement yielded no detectable signal whatsoever (Fig. 5B, *left*, and 5C, *left*) suggesting that, even when bound at the septin collar, the N terminus of Hsl1 (which contains its catalytic domain) lies very far away from the C termini of every septin. We next tested an N-terminally β10-tagged version of the 611-950 fragment from which the NLS and the D and KEN boxes had been mutationally inactivated against the β11-tagged versions of the five mitotic septins. Satisfyingly, under these conditions, a readily detectable signal was observed only between β10-611-950 and Cdc12-β11 in the majority of cells (Fig. 5B, *middle*), and more occasional and weaker interaction with Cdc3-β11 (Fig. 5C, *middle*). Third, we examined the interaction of the same N-terminally β10-tagged NLS-less and D- and KEN box-less 611-950 fragment to which the KA1 (residues 1245-1518 of Hsl1) was appended against the β11-tagged versions of the five mitotic septins. We again observed strongest interaction with Cdc12-β11, somewhat less robust interaction with Cdc3-β11 and Cdc10-β11, and much less with Cdc11-β11 and Shs1-β11 (Fig. 5C, *right*, and *5C, right*).

To maximize the likelihood of capturing the 611-950 fragment or 611-950; 1245-1518

fragment interaction with a septin(s), linkers of maximal length were used (the β10 tag was tethered by a 32-residue linker and the β11 tag was appended to a 33-residue linker). We reasoned that we could make the test of the subunit binding specificity of Hsl1 more stringent by systematically shortening the linker length in both the 611-950; 1245-1518 fragment and the septin constructs and reassessing the resulting readouts. Reassuringly, using this approach, there was a clearcut trend in the 60 diploids constructed for this set of analyses (Fig. 5D). As the linker lengths were shortened, the robustness of the output signal was progressively strengthened for the interaction of the β10-611-950; 1245-1518 fragment with Cdc12-β11 and Cdc3-β11 and correspondingly greatly diminished for its interaction with the other three septin-β11 constructs. Hence, it is clear that the septin-binding element in Hsl1 associates primarily with Cdc12 and Cdc3, a specificity not previously characterized.

Use of the tripartite split-GFP method to examine other bud neck-associated proteins

There are scores of cellular proteins that reportedly localize exclusively or to a detectable degree at the bud neck and do so with different spatiotemporal dynamics (Gladfelter et al., 2001; McMurray and Thorner, 2009; Finnigan et al., 2015a). For the majority of these proteins, there is little or no information about whether they localize to the bud neck because they directly bind to a septin(s) there, or not. Hence, as a final test of the usefulness of the tripartite split-GFP assay, we examined three bud neck-associated proteins whose capacity to physically associate with specific septins has, to our knowledge, not yet been definitively characterized.

The first such protein we examined was a poorly studied bud neck-localized factor, Nis1 (407 residues), whose purported ability to physically associate with septin Shs1 is based mainly on a two-hybrid interaction reported in a single study (Iwase and Toh-e, 2001). In our hands, Nis1-eGFP expressed under its endogenous promoter in a strain co-expressing Cdc10-mCh does not co-localize with the septin collar. In cells with small or large buds, Nis1 is found just adjacent to the division site in a small patch (Fig. 5A, *top*); in cells undergoing cytokinesis, Nis1 is localized *between* the split septin rings (Fig. 5A, *bottom*). An eGFP-Nis1 construct shows the

identical localization pattern (G. Finnigan, unpublished results). Nonetheless, to determine whether the tripartite split-GFP system could detect any transient or weak interaction of Nis1 with any septin during cytokinesis (when Nis1 is localized between the split septin rings), we tested Nis1-β11 against β10-tagged versions of all five septins (Fig. 6B) and also β10-Nis1 against β11-tagged versions of all five septins (Fig. 6D) (where, to maximize the likelihood of detection, the N-terminal β10 tag was tethered by an 18-residue linker and β11 tag was appended via a 33-residue linker). We carefully examined all cells, but especially dividing cells that were actively undergoing cytokinesis (*i.e.*, contained a split double ring marked by Cdc10-mCh or Cdc11-mCh). In neither arrangement (Nis1-β11 and β10-tagged septins or β10-Nis1 and β11-tagged septins) did we detect any signal above the intrinsic background fluorescence (Fig. 6C and 6E). We conclude, therefore, that Nis1 is sequestered between the split septins, but does not make direct contact with any septin there. Thus, recruitment of Nis1 to this location is not mediated by its binding to any septin. We cannot rule out, however, that the β10 or β11 tags (and/or the unstructured linkers) perturb the ability of Nis1 to interact with a septin, but such a concern seems unlikely given that both eGFP-Nis1 and Nis1-eGFP, which are fused to much bulkier tags, display exclusive localization within the split septin rings at the bud neck.

The second bud neck-associated factor we examined was Bud4, a large (1447 residues) protein involved in bud site selection that is the putative yeast analog of mammalian anillin (Eluere et al., 2012; Kang et al., 2013; Wu et al., 2015). Although prior work has provided both genetic and biochemical evidence indicating that Bud4 makes direct contact with septins, the subunit specificity of its interaction has not previously been defined. However, as for Hsl1 (Finnigan et al., 2016), domain scans across full-length Bud4 have revealed a minimal domain (residues 623-774) that is largely sufficient for localization to the septin collar (Wu et al., 2015). Therefore, and as for Hsl1, we focused our analysis to this previously identified, putative septin-binding domain of Bud4. Indeed, in our hands, a Bud4(623-774)-eGFP construct strongly co-localized with the septin collar marked with Cdc10-mCh (although a detectable amount of this

fragment was also found in the nucleus) (Fig. 7A). Tellingly, when Bud4(623-774)-β11 was tested against β10-tagged version of all five mitotic septins, prominent signals were observed with β10-Cdc3, β10-Cdc11 and β10-Shs1 (Figs. 7B and 7C), confirming that this region of Bud4 is indeed able to make intimate physical contact with these septins at the bud neck.

The third bud neck-localized protein we interrogated was Hof1, an F-BAR domain-containing protein involved in membrane curvature and actomyosin ring coordination during cytokinesis (Nishihama et al., 2009; Meitinger et al., 2011; Meitinger et al., 2013; Oh et al., 2013). As for Bud4, prior genetic and biochemical findings indicate that Hof1 makes direct contact with septins at the bud neck, but its subunit selectivity was not clearly identified previously. Like Bud4, domain scans across full-length Hof1 (669 residues) have delineated a minimal domain (residues 293-356) that is (partially) sufficient for localization to the septin collar (Meitinger et al., 2013). In our hands, an eGFP-Hof1(293-356) construct was found mainly in the cytosol, but did localize detectably, although only rather weakly, at the bud neck, congruent with Cdc10-mCh (Fig. 7D). However, consistent with the capacity of the tripartite split-GFP method to capture even weak or transient interactions, when Hof1(293-356)-β11 was tested against β10-tagged version of all five mitotic septins, robust signals were observed with β10-Cdc12, β10-Cdc10 and β10-Cdc3 (Figs. 7E and 7F), confirming that this region of Hof1 is indeed able to make intimate physical contact with these septins at the bud neck.

Bud4(623-774)-β11 interacted with both terminal subunits of the hetero-octamer (β10-Cdc11 and β10-Shs1), but also with β10-Cdc3; by contrast, Hof1(293-355)-β11 interacted with β10-β10-Cdc12 and β10-Cdc10, but also with β10-Cdc3. Cdc3 is perhaps a bit more "promiscuous" in its ability to interact with other proteins docked at the septin collar, as judged by the tripartite split-GFP method, because its long N-terminal extension (Fig. S1B) may allow for greater flexibility and a longer "reach." Importantly, however, when we swapped the tags, and tested β10-Bud4(623-774) or β10-Hof1(293-356) against β11-tagged version of all five mitotic septins, no fluorescence signal was generated by any combination (data not shown), strongly

suggesting that the septin-binding domains of Bud4 and Hof1 have a very strong preference for associating with the N-terminal "face" of their target septins in the hetero-octamer. We observed the converse with the septin-binding domain of Hsl1; we only observed robust fluorescent signals when β10-Hsl1(611-950) or β10-Hsl1(611-950; 1245-1518) were combined with β11-tagged version of all five mitotic septins (Fig. 5), indicating that Hsl1 prefers association with the C-terminal ends of the septins in the hetero-octamer.

DISCUSSION

We demonstrated here that the tripartite split-GFP system (Cabantous et al., 2013) is a reliable, *in vivo* protein-protein interaction sensor in *S. cerevisiae* cells, where this technology had not previously been applied. This method permitted successful interrogation of protein-protein associations *in situ* under near-native conditions at endogenous levels of expression. Any proteins examined are present in their normal modification state and in their natural intracellular location and milieu when their ability to physically interact is assessed. Given their small size, the tags (20-21 residues) have a minimal effect on the solubility and other behaviors of the tagged proteins, whose interaction was readily detectable even in diploid cells where a WT copy of each tagged partner was also present (see Fig. S1).

Regardless of when and where the β10-tagged and β11-tagged proteins interact, the readout is only generated upon expression of the complementary otherwise non-fluorescent eGFPβ1-9 barrel. Hence, background fluorescence is minimal. This arrangement allows for temporal control. For example, two β10- and β11-tagged proteins that interact transiently only in a particular phase of the cell cycle could be revealed, in principle, by arresting cells at different cell cycle stages with drugs or mutants, and then inducing expression of the eGFPβ1-9 barrel. This arrangement also allows for spatial control. For example, to interrogate interaction of only PM-localized β10- and β11-tagged proteins, one could use as the detector a modified eGFPβ1-9 barrel targeted to the PM by an N-terminal myristoylation sequence or a C-terminal CaaX box. Furthermore, by generating libraries of *MAT***a** cells expressing β10-tagged derivatives of every yeast gene and corresponding libraries of *MAT*α cells expressing β11-tagged derivatives of every yeast gene (and vice versa), simple crosses among these collections and examination of the resulting diploids by fluorescence microscopy after induction of the eGFPβ1-9 barrel should, in theory, provide a independent means to generate a new global protein interactome map for the entire *S. cerevisiae* genome to expand upon and complement currently available data.

We addressed, first, interrelationships among the subunits in the linear, apolar septin

hetero-octamer (Bertin et al., 2008). However, Cdc11-capped hetero-octameric rods polymerize end-to-end and also associate in register in a highly cooperative manner laterally (via cross-filament interaction mediated by coiled coil formation between the C termini of Cdc3 and Cdc12), to form long paired filaments (Versele et al., 2004; Bertin et al., 2008; McMurray et al., 2011). Similarly, Shs1-capped hetero-octamers self-associate into arcs, spirals and rings (Garcia et al., 2011). Together, these septin complexes form higher-order arrays of various geometries *in vivo* (Rodal et al., 2005; Bertin et al., 2012; Ong et al., 2014). Hence, one potential concern in interpreting the readout generated for septin-septin interactions using the tripartite split-GFP approach was that the observed fluorescent signal could arise from an amalgam of interactions occurring at four distinct levels of organization: (i) within hetero-octamers; (ii) across the filaments within a pair; (iii) between neighboring pairs of filaments; and/or, (iv) among higher-order assemblies in larger superstructures (Bertin et al., 2012).

We found, however, that the occurrence and intensity of the fluorescent signal observed between pairs of septins largely mirrors the known subunit order within the hetero-octamer. Thus, our observations indicate that the tripartite split-GFP method mainly measures intimate short-range physical contacts. Even when the linkers tethering the β10 and β11 tags to their respective septins were extended, authentic nearest-neighbor subunit pairings generally yielded much more robust outputs than any longer range, non-nearest neighbor interactions. Nonetheless, by increasing linker length, we could begin to detect such readouts. For example, in the hetero-octamer, any given Cdc10 is adjacent to another Cdc10 and to Cdc3 and gives a very strong signal with either partner; yet, at the longest linker lengths we used, interaction (albeit much weaker) of Cdc10 with Cdc12 (the next subunit over from Cdc3) was detectable. Hence, systematic variation of the linkers that tether the β10 and β11 tags to their respective proteins provides a tunable "molecular ruler" for gauging *in vivo* the relative distances among protein components in a complex. The globular domain of a septin is ~4 nm in diameter (Bertin et al., 2008); we estimate, therefore, that the longest linkers we used interrogated

conformational space more than 10 nm away from their point of attachment. Thus, the shorter the linker length, the more stringent the distance requirements for interaction; conversely, the longer the linker length, the more promiscuous the associations that will be detected, up to a point. We saw the latter behavior for β10-Cdc3, presumably because it has a much longer N-terminal extension than any other mitotic septin. Conversely, we generally encountered less robust signals with β10-Cdc11 and β10-Shs1 because both have extremely short N-terminal extensions that include, just downstream, a tract of basic residues. By binding to PtdIns4,5P_2 on the inner leaflet of the PM, these tracts in Cdc11, Shs1 and Cdc10 contribute to the tight association between septin filaments and the PM and thus to septin function (Bertin et al., 2010; Bridges et al., 2014; Finnigan et al., 2015b). Membrane association may partially occlude access to the N termini of these septins.

A primary purpose for implementing the tripartite split-GFP system was to address three questions about the ~100 proteins that reportedly localize (in whole or in part) at the bud neck (either seemingly congruent with or otherwise in close proximity to the septin collar) at some point during cell cycle progression (Gladfelter et al., 2001; McMurray and Thorner, 2009; Finnigan et al., 2015a): (i) which of these proteins actually binds directly to a septin and which are recruited to the bud neck by less direct mechanisms; (ii) for proteins that associate intimately, do they contact a specific septin subunit, thereby providing insight into how these septin-binding proteins are organized at the bud neck; and, (iii) for septin-binding proteins, does this approach allow for reliable parsing of the sequence elements necessary and sufficient for their septin interaction.

Examination of full-length (448 residues) Bni5, known to interact directly with Cdc11 and Shs1 (Lee et al., 2002; Booth et al., 2015; Finnigan et al., 2015a; Patasi et al., 2015), validated that the tripartite split-GFP method yields the same conclusion. Consistent with other evidence that the C-terminal end of Bni5 is required for its function (Finnigan et al., 2015a), Bni5-β11 interacted exclusively with N-terminally β10-tagged Cdc11 and Shs1 and no other septin. In

agreement with structure predictions that Bni5 is an elongated, highly α-helical protein, β10-Bni5 exhibited a longer "reach", yielding a readily detectable fluorescent signal with every C-terminally β11-tagged septin. Thus, this method provides a certain degree of insight about how septin-binding proteins are oriented when they dock on the septin collar (Fig. 8).

To verify that the tripartite split-GFP method reports interaction of authentic septin-binding domains, we turned to the much larger (1518 residues), multi-domain, septin collar-binding protein Hsl1. An internal segment of Hsl1 (residues 611-950) is both necessary and sufficient for targeting the enzyme to the septin collar *in vivo* and for direct binding to septin filaments *in vitro* (Finnigan et al., 2016). We found that the β10-611-950 fragment exhibited a marked preference for association with C-terminally β11-tagged Cdc12 and Cdc3, whereas 611-950-β11 yielded no detectable interaction with any N-terminally β10-tagged septin (Fig. 8). Aside from confirming that this Hsl1 segment associates directly with the septin collar, the tripartite split-GFP method revealed that it docks via its N-terminal end to the C-terminal ends of Cdc12 and Cdc3. Thus, this technique shed light on how a septin-binding domain within a larger septin-binding protein engages the septin collar. N-terminally β10-tagged full-length Hsl1 did not yield a detectable signal with any C-terminally β11-tagged septin, suggesting that, when bound to the septin collar, the N-terminal kinase domain likely faces away from the septin filaments and projects into the cytosol at the bud neck. C-terminally β11-tagged full-length Hsl1 also did not yield a detectable signal with any N-terminally β10-tagged septin. Given that the β11 tag is located downstream of the PtdSer-binding C-terminal KA1 domain, it was likely buried against the surface of the PM and, hence, inaccessible.

Although smaller than Bni5, neither Nis1-β11 combined with β10-tagged septins nor β10-Nis1 combined with β11-tagged septins displayed any signal above background, suggesting that Nis1 is located at the bud neck during cytokinesis by physical trapping between the two septin rings, not by direct binding to any septin. For Bud4 and Hof1, prior deletion analysis and fragment scanning had identified segments that appear both necessary and sufficient for their

septin association. However, whether Bud4 or Hof1 binding have any septin subunit specificity or any preference for which "face" of a septin filament they occupy had not been determined. When C-terminally β11-tagged, the Bud4 septin-binding domain interacted preferentially with β10-Cdc11 and β10-Shs1 (Fig. 8), whereas, when N-terminal β10-tagged, it did not interact detectably with any septin-β11. Similarly, when C-terminally β11-tagged, the Hof1 septin-binding element interacted preferentially with β10-Cdc12 and β10-Cdc10, but, when N-terminal β10-tagged, it did not interact detectably with any septin-β11 (Fig. 8). Thus, the septin-binding domains in both Bud4 and Hof1 preferentially associate with distinct septins and do so via the N-terminal "face" of the septin filaments at the bud neck.

PM binding via its C-terminal KA1 domain greatly potentiates the ability of the Hsl1 septin-binding region to engage the septin collar *in vivo* (Finnigan et al., 2016). Likewise, Bud4 has a C-terminal, phosphoinositide-binding pleckstrin homology domain (residues 1305-1447) (Gallego et al., 2010; Kang et al., 2013; Wu et al., 2015). Similarly, Hof1 contains an apparent N-terminal F-BAR domain (residues 1-280) (Aspenström, 2009) required for its recruitment to the PM (Meitinger et al., 2013; Oh et al., 2013). Thus, synergistic action of both PM-binding motifs and septin-binding elements in certain bud neck-localized proteins presumably coordinates their function with processes that influence the lipid composition of the PM.

Whether the subunit arrangement within septin hetero-octamers (and in the higher-order structures built from them) arose due to evolutionary selection for efficient assembly or as a means to more effectively dictate positioning of associated septin-binding proteins (or both) has been an open question. There is some evidence for the latter. Localization of Bni5 to the terminal subunits (Cdc11 and Shs1) of the hetero-octamer is required for its function (Finnigan et al., 2015a). Artificially tethering Bni5 to that location (via gene fusions or nanobody-mediated recruitment) suffices, whereas Bni5 tethered by the same means to Cdc10 at the center of the hetero-octamer is unable to function (Finnigan et al., 2015a). Whether the subunit-specific position of any other septin-associated protein is crucial for its function has, to our knowledge,

not yet been explored. Such information is important to understand how these factors exert their physiological actions. Most studies reporting interaction between a septin and a cellular protein have not systematically examined specificity *per se*, for example: (i) testing a two-hybrid interaction between a protein of interest and one or two "representative" septin subunits rather than with all five mitotic septins (Nagaraj et al., 2008); (ii) screening for synthetic lethality with mutations in one or a few septins rather than all five subunits (Costanzo et al., 2010); (iii) co-immunoprecipitation or pull-down of a protein of interest with only a single subunit rather than all five septins (Meitinger et al., 2013; Renz et al., 2016); (iv) scoring the phenotype of a fusion of a protein of interest to the C-terminus of one septin rather than constructing and testing fusions to all five (King et al., 2012; Kang et al., 2016); or, (v) using a fluorescent PCA assay that pairs a tagged protein of interest with a single tagged septin rather than with each of the five septins (Renz et al., 2016). By contrast, the tripartite split-GFP method allows for facile assessment of the potential interaction between any two proteins of interest. In our study, we focused on the ability to detect initial protein-protein interactions because of the potentially complicating effects of long-term stabilization of dynamic protein-protein associations that arises from tethering the two proteins together "irreversibly" via formation of reconstituted eGFP.

Yeast strains and plasmids

The yeast strains used in this study are listed in Table 1. Standard molecular biology techniques and protocols were followed (Sambrook and Russell, 2001). The tripartite split-GFP components we utilized are based on reagents described in detail elsewhere (Cabantous et al., 2013). Two gene constructs were synthesized (Genscript, Piscataway, NJ) with optimized yeast codon usage bias: (i) the evolved e*GFPβ1-9* variant (Cabantous et al., 2013); and, (ii) the β10 and β11 strands of the evolved eGFP variant (Cabantous et al., 2013) in the form of a construct consisting of the sequence *SpeI*::*β10*::*Linker(32)*::*SacI*::*Linker(33)*::*β11*::*ADH(t)*::*NotI*. To generate the C-terminally tagged versions of the proteins examined, a common methodology was used that involves a PCR-based *in vivo* ligation and homologous recombination method in yeast (Finnigan and Thorner, 2015). In brief, plasmids were assembled that contain the native promoter region (usually 500 bps of the upstream 5'-UTR), the ORF of the gene of interest, a linker of either 0, 10, 20, 33 or 43 residues, the C-terminal β11 sequence, the *ADH1* terminator, and an MX-based drug cassette (Goldstein and McCusker, 1999). Each construct was confirmed via DNA sequencing. Next, the entire cassette was PCR amplified using the plasmid DNA as the template, treated with *Dpn*I, and introduced by DNA-mediated transformation into yeast to replace a chromosomal deletion of the gene of interest. To maintain viability for integration of the tagged version of any essential gene, the cells also harbored a *URA3*-based covering plasmid carrying a WT copy of the cognate gene, which was then removed by selection on medium containing 5-fluoro-orotic acid (5-FOA). Proper integration was confirmed by diagnostic PCRs on isolated chromosomal DNA and, when appropriate, Sanger sequencing of the manipulated loci (Univ. of California, Berkeley Barker Hall Sequencing Facility).

To generate the N-terminally tagged versions of the proteins examined, a modified protocol was used. First, the promoter (present on a pRS315 plasmid) was tagged downstream with the *β10::Linker(32)::SacI::Linker(33)::β11:::ADH1(t)::Kan*^{R} sequence using *in vivo* ligation. Second, the promoter::*β10::Linker(32)* segment of the construct was subcloned to a separate pRS315

vector using a unique restriction site upstream of the promoter (typically *Not1* or *SpeI*) and the unique *SacI* site. Third, a second round of *in vivo* assembly was performed to fuse the ORF of the gene of interest to the *promoter::β10::Linker(32)* element (with either the full-length linker or truncations of it resulting in linkers of 18 or 5 residues), followed by the *ADH1* terminator and an MX-based drug resistance cassette. Fourth, the entire cassette was PCR amplified and integrated into the genome, as describe above. For insertion into the genome of either *CDC10::mCherry::SpHIS5* or *CDC11::mCherry::SpHIS5* in the strains containing β10- or β11-tagged gene product, the mCherry-containing construct was PCR amplified using primers present in the flanking UTR (+/-300 for *CDC11* and +/-500 for *CDC10*) and the resulting product was introduced by DNA-meditated transformation and the desired derivatives selected on SD-His medium. For tagging of *CDC19*, *GPP1*, *HSP82*, *PGK1* and *TPI1*, otherwise WT yeast (BY4741) were transformed with either full-length eGFP or the β11 tag cassette flanked by appropriate PCR generated segments of homology to the cognate chromosomal locus. DNA isolated from each resulting integrant was amplified with a high-fidelity polymerase and sequenced to verify correct construction. All DNA plasmids (Table 2) were constructed using *in vivo* ligation in yeast and were confirmed both by diagnostic PCR and by DNA sequencing of the entire coding region of each gene fusion and all junctions to UTR sequence.

Culture conditions

Yeast were grown in rich (YPD) medium (2% peptone, 1% yeast extract, 2% dextrose) or in synthetic medium. The drop-out medium contained the proper mixture of amino acids to maintain selection for all markers and/or plasmids and, as the carbon source, either 2% dextrose, 2% raffinose-0.2% sucrose, or 2% galactose, as appropriate. During the construction of any strain that involved introduction of a tagged version of an essential septin gene, the cells harbored a *URA3*-marked covering plasmid expressing the corresponding WT septin gene. Only after confirmation of the integrated allele, the covering plasmid was removed by two successive rounds of selection at 30°C on medium containing 5-FOA (Oakwood Products Inc., West

Columbia, SC) (final concentration of 0.5 mg/mL; heated for at least 30 min to 70°C and filter sterilized, not autoclaved). All of the haploid strains expressing integrated tagged copies of either septin subunits (or bud neck-localized proteins) were confirmed to be viable at 30°C on medium containing 5-FOA (for essential subunits) before they were used for mating and the selection of the resulting diploids. Conditions for diploid isolation involved two successive rounds of growth under conditions selection for both the *mCherry::SpHIS5*-marked septin introduced from the *MAT*α partner (*e.g.*, GFY-1794) and the *LEU2*-marked plasmid carrying the *GAL1/10$_{prom}$::GFPβ1-9* introduced from the *MAT***a** partner (*e.g.*, GFY-1851). For the constructs involving Bud4 and Hof1, a modified diploid selection protocol was used. Each mating type received one of two plasmids expressing either (i) *GAL1/10$_{prom}$::GFPβ1-9* (*URA3*-marked) or (ii) *BUD4::β11 or HOF1::β11* (*LEU2*-marked). Diploids then were selected and propagated on SD-Ura-Leu medium.

Fluorescence microscopy and quantification

For imaging of strains not containing any plasmids (*e.g.*, GFY-2034), yeast were grown overnight at 30°C in YPD to saturation, back-diluted in 10 mL of fresh YPD to an $A_{600\ nm}$ of 0.25 and grown for an additional 4-5 h to an $A_{600\ nm}$ ~1. Cells were harvested, washed with water, placed on a glass slide with a cover slip, and imaged within 5 min. Diploid strains were grown overnight to saturation at 30°C in synthetic medium lacking both Leu and His (to maintain selection) with 2% raffinose-0.2% sucrose. The cultures were back-diluted to an $A_{600\ nm}$ of 0.3-0.4 in the same medium containing 2% galactose as the carbon source (to induce GFPβ1-9 expression) and grown for an additional 4.5-5 h at 30°C before being washed and imaged.

Yeast cells were examined using an Olympus BH-2 upright fluorescence microscope (Olympus, Toyko, Japan) with a 100x objective lens, equipped with an eGFP 49002 cut-off filter™ (Chroma Technology Corp, Bellows Falls, VT) that allows for 94.65% transmission at 488 nm (the excitation maximum for eGFP) and 97.69% transmission at 509 nm (the emission maximum for eGFP) and an mCherry/Texas Red filter (Chroma) that allows for 97.82%

transmission at 579 nm (mCherry has excitation max of 587 nm) and 97.84% transmission at 610 nm (the emission maximum for mCherry). A SOLO™ light source (Lumencore, Beaverton, OR), a CoolSNAP MYO™ CCD camera, and Micro-Manager software (Edelstein et al., 2010) were used to record the images. Post-processing and analysis of images were done using ImageJ (National Institute of Health). All images were treated identically and rescaled together. For clarity, the periphery of yeast cells was labeled using white dotted lines from an overexposed image or a corresponding DIC (differential interference contrast) image. Unless otherwise indicated, all images were taken for the same exposure time and using the same light source power level.

The results described are average values for each diploid strain derived from experiments conducted in triplicate. For quantification of the percentage of the cell population that displayed a detectable reconstituted eGFP signal at the bud neck, 25 to 100 cells in separate fields were scored and divided by the total number of cells in the same fields that exhibited a detectable mCherry signal (i.e., had an obvious septin collar). For quantification of the pixel intensity of the eGFP fluorescence at the bud neck, the box tool in ImageJ was used to carefully outline the bud neck in 25 to 100 cells that also clearly displayed a septin collar (as judged by the mCherry signal) and the average pixel intensity (with standard error of that mean) was calculated (after subtracting the average background fluorescence in any given image from each measurement taken in the same image). The average background fluorescence was determined from assessing using the box tool the pixel intensity of an equivalent area of five randomly-chosen regions of each image that did not contain any cells. It should be noted that this average background fluorescence is distinct from the pixel intensity present at the bud neck of otherwise wild-type yeast due to the intrinsic fluorescence of cellular components (approximately 35-40, displayed as the red dotted line in our bar graphs).

For the experiments involving Hsl1 or Bni5, cells displaying a split septin ring (as judged by the mCherry signal) were excluded from the analysis because native Hsl1 is displaced from the

bud neck at the onset of cytokinesis by its APC-mediated degradation (Burton and Solomon, 2000; Finnigan et al., 2016) and Bni5 is also ejected from this location prior to cytokinesis (Lee et al., 2002; Finnigan et al., 2015a). Conversely, for quantification of Nis1 at the bud neck, only budded cells that displayed a clear split septin ring were included as native Nis1 is not present at the bud neck until cytokinesis (Fig. 5A).

ACKNOWLEDGMENTS

We would like to thank the other members of the Thorner Lab for useful suggestions and Geoffrey Waldo (Los Alamos National Laboratory) for providing invaluable research materials. This work was supported by a Postdoctoral Fellowship from the Adolph C. and Mary Sprague Miller Institute for Basic Research in Science (to G.C.F.), by National Institutes of Health Research Grants GM21841 (to J.T.) and GM101314 (to J.T. and colleague Eva Nogales). All of the authors declare no competing financial interests.

LITERATURE CITED

Aspenström, P. (2009). Roles of F-BAR/PCH proteins in the regulation of membrane dynamics and actin reorganization. Int. Rev. Cell Mol. Biol. *272*, 1-31.

Bertin, A., McMurray, M.A., Grob, P., Park, S.S., Garcia, G., 3rd, Patanwala, I., Ng, H.L., Alber, T., Thorner, J., and Nogales, E. (2008). *Saccharomyces cerevisiae* septins: supramolecular organization of heterooligomers and the mechanism of filament assembly. Proc. Natl. Acad. Sci. USA *105*, 8274-8279.

Bertin, A., McMurray, M.A., Pierson, J., Thai, L., McDonald, K.L., Zehr, E.A., Garcia, G., 3rd, Peters, P., Thorner, J., and Nogales, E. (2012). Three-dimensional ultrastructure of the septin filament network in *Saccharomyces cerevisiae*. Mol. Biol. Cell *23*, 423-432.

Bertin, A., McMurray, M.A., Thai, L., Garcia, G., 3rd, Votin, V., Grob, P., Allyn, T., Thorner, J., and Nogales, E. (2010). Phosphatidylinositol-4,5-bisphosphate promotes budding yeast septin filament assembly and organization. J. Mol. Biol. *404*, 711-731.

Bi, E., and Park, H.O. (2012). Cell polarization and cytokinesis in budding yeast. Genetics *191*, 347-387.

Booth, E.A., Vane, E.W., Dovala, D., and Thorner, J. (2015). A Förster resonance energy transfer (FRET)-based system provides insight into the ordered assembly of yeast septin hetero-octamers. J. Biol. Chem. *290*, 28388-28401.

Brachmann, C.B., Davies, A., Cost, G.J., Caputo, E., Li, J., Hieter, P., and Boeke, J.D. (1998). Designer deletion strains derived from *Saccharomyces cerevisiae* S288C: a useful set of strains and plasmids for PCR-mediated gene disruption and other applications. Yeast *14*, 115-132.

Brausemann, A., Gerhardt, S., Schott, A.K., Einsle, O., Große-Berkenbusch, A., Johnsson, N., and Gronemeyer, T. (2016). Crystal structure of Cdc11, a septin subunit from *Saccharomyces cerevisiae*. J. Struct. Biol. *193*, 157-161.

Bridges, A.A., and Gladfelter, A.S. (2015). Septin form and function at the cell cortex. J. Biol. Chem. *290*, 17173-17180.

Bridges, A.A., Zhang, H., Mehta, S.B., Occhipinti, P., Tani, T., and Gladfelter, A.S. (2014). Septin assemblies form by diffusion-driven annealing on membranes. Proc. Natl. Acad. Sci. USA *111*, 2146-2151.

Burton, J.L., and Solomon, M.J. (2000). Hsl1p, a Swe1p inhibitor, is degraded via the anaphase-promoting complex. Mol. Cell. Biol. *20*, 4614-4625.

Burton, J.L., and Solomon, M.J. (2001). D box and KEN box motifs in budding yeast Hsl1p are required for APC-mediated degradation and direct binding to Cdc20p and Cdh1p. Genes

Dev. *15*, 2381-2395.

Byers, B., and Goetsch, L. (1976). A highly ordered ring of membrane-associated filaments in budding yeast. J. Cell Biol. *69*, 717-721.

Cabantous, S., Nguyen, H.B., Pedelacq, J.D., Koraichi, F., Chaudhary, A., Ganguly, K., Lockard, M.A., Favre, G., Terwilliger, T.C., and Waldo, G.S. (2013). A new protein-protein interaction sensor based on tripartite split-GFP association. Sci. Rep. *3*, 2854.

Carroll, C.W., Altman, R., Schieltz, D., Yates, J.R., and Kellogg, D. (1998). The septins are required for the mitosis-specific activation of the Gin4 kinase. J. Cell Biol. *143*, 709-717.

Cid, V.J., Adamíková, L., Cenamor, R., Molina, M., Sánchez, M., and Nombela, C. (1998). Cell integrity and morphogenesis in a budding yeast septin mutant. Microbiology *144*, 3463-3474.

Costanzo, M., Baryshnikova, A., Bellay, J., Kim, Y., Spear, E.D., Sevier, C.S., Ding, H., Koh, J.L., Toufighi, K., Mostafavi, S.*, et al.* (2010). The genetic landscape of a cell. Science *327*, 425-431.

Drees, B., L., Sundin, B., Brazeau, E., Caviston, J.P., Chen, G.C., Guo, W., Kozminski, K.G., Lau, M.W., Moskow, J.J., Tong, A.*, et al.* (2001). A protein interaction map for cell polarity development. J Cell Biol *154*, 549-571.

Dunkler, A., Rosler, R., Kestler, H.A., Moreno-Andres, D., and Johnsson, N. (2015). SPLIFF: A single-cell method to map protein-protein interactions in time and space. Methods Mol. Biol. *1346*, 151-168.

Edelstein, A., Amodaj, N., Hoover, K., Vale, R., and Stuurman, N. (2010). Computer control of microscopes using microManager. Current protocols in molecular biology (Ausubel FM *et al*., eds.), *Chapter 14*, Unit 14.20.

Eluere, R., Varlet, I., Bernadac, A., and Simon, M.N. (2012). Cdk and the anillin homolog Bud4 define a new pathway regulating septin organization in yeast. Cell Cycle *11*, 151-158.

Ewers, H., Tada, T., Petersen, J.D., Racz, B., Sheng, M., and Choquet, D. (2014). A septin-dependent diffusion barrier at dendritic spine necks. PloS One *9*, e113916.

Fang, X., Luo, J., Nishihama, R., Wloka, C., Dravis, C., Travaglia, M., Iwase, M., Vallen, E.A., and Bi, E. (2010). Biphasic targeting and cleavage furrow ingression directed by the tail of a myosin II. J. Cell Biol. *191*, 1333-1350.

Farkasovsky, M., Herter, P., Voss, B., and Wittinghofer, A. (2005). Nucleotide binding and filament assembly of recombinant yeast septin complexes. Biol Chem *386*, 643-656.

Finnigan, G.C., Booth, E.A., Duvalyan, A., Liao, E.N., and Thorner, J. (2015a). The carboxy-terminal tails of septins Cdc11 and Shs1 recruit myosin-II binding factor Bni5 to the bud

neck in *Saccharomyces cerevisiae*. Genetics *200*, 821-840.

Finnigan, G.C., Sterling, S.M., Duvalyan, A., Liao, E.N., Sargsyan, A., Garcia, G.r., Nogales, E., and Thorner, J. (2016). Coordinate action of distinct sequence elements localizes checkpoint kinase Hsl1 to the septin collar at the bud neck in *Saccharomyces cerevisiae.* Mol. Biol. Cell [Epub ahead of print, 18 May 2016].

Finnigan, G.C., Takagi, J., Cho, C., and Thorner, J. (2015b). Comprehensive genetic analysis of paralogous terminal septin subunits Shs1 and Cdc11 in *Saccharomyces cerevisiae*. Genetics *200*, 841-861.

Finnigan, G.C., and Thorner, J. (2015). Complex in vivo ligation using homologous recombination and high-efficiency plasmid rescue from *Saccharomyces cerevisiae*. Bio-protocol *5*, e1521.

Fung, K.Y., Dai, L., and Trimble, W.S. (2014). Cell and molecular biology of septins. Intt. Rev. Cell Mol. Biol. *310*, 289-339.

Gallego, O., Betts, M.J., Gvozdenovic-Jeremic, J., Maeda, K., Matetzki, C., Aguilar-Gurrieri, C., Beltran-Alvarez, P., Bonn, S., Fernández-Tornero, C., Jensen, L.J.*, et al.* (2010). A systematic screen for protein-lipid interactions in *Saccharomyces cerevisiae*. Mol. Syst. Biol. *6*, 430.431-430.415.

Garcia, G., 3rd, Bertin, A., Li, Z., Song, Y., McMurray, M.A., Thorner, J., and Nogales, E. (2011). Subunit-dependent modulation of septin assembly: budding yeast septin Shs1 promotes ring and gauze formation. J. Cell Biol. *195*, 993-1004.

Gladfelter, A.S., Pringle, J.R., and Lew, D.J. (2001). The septin cortex at the yeast mother-bud neck. Curr. Opin. Microbiol. *4*, 681-689.

Goldstein, A.L., and McCusker, J.H. (1999). Three new dominant drug resistance cassettes for gene disruption in *Saccharomyces cerevisiae*. Yeast *15*, 1541-1553.

Haarer, B.K., and Pringle, J.R. (1987). Immunofluorescence localization of the *Saccharomyces cerevisiae CDC12* gene product to the vicinity of the 10-nm filaments in the mother-bud neck. Mol. Cell. Biol. *7*, 3678-3687.

Hall, P.A., and Russell, S.E. (2012). Mammalian septins: dynamic heteromers with roles in cellular morphogenesis and compartmentalization. J. Pathol. *226*, 287-299.

Hartwell, L.H. (1971). Genetic control of the cell division cycle in yeast. IV. Genes controlling bud emergence and cytokinesis. Exp. Cell Res. *69*, 265-276.

Hartwell, L.H., Culotti, J., Pringle, J.R., and Reid, B.J. (1974). Genetic control of the cell division cycle in yeast. Science *183*, 46-51.

Huh, W.K., Falvo, J.V., Gerke, L.C., Carroll, A.S., Howson, R.W., Weissman, J.S., and O'Shea,

E.K. (2003). Global analysis of protein localization in budding yeast. Nature *425*, 686-691.

Iwase, M., Luo, J., Bi, E., and Toh-e, A. (2007). Shs1 plays separable roles in septin organization and cytokinesis in *Saccharomyces cerevisiae*. Genetics *177*, 215-229.

Iwase, M., and Toh-e, A. (2001). Nis1 encoded by YNL078W: a new neck protein of *Saccharomyces cerevisiae*. Genes & genetic systems *76*, 335-343.

Kang, H., Tsygankov, D., and Lew, D.J. (2016). Sensing a bud in the yeast morphogenesis checkpoint: a role for Elm1. Mol. Biol. Cell [Epub ahead of print, 6 April 2016]

Kang, P.J., Hood-DeGrenier, J.K., and Park, H.O. (2013). Coupling of septins to the axial landmark by Bud4 in budding yeast. J. Cell Sci. *126*, 1218-1226.

Kerppola, T.K. (2009). Visualization of molecular interactions using bimolecular fluorescence complementation analysis: characteristics of protein fragment complementation. Chem. Soc. Rev. *38*, 2876-2886.

King, K., Jin, M., and Lew, D. (2012). Roles of Hsl1p and Hsl7p in Swe1p degradation: beyond septin tethering. Eukaryot. Cell *11*, 1496-1502.

Kumar, A., Agarwal, S., Heyman, J.A., Matson, S., Heidtman, M., Piccirillo, S., Umansky, L., Drawid, A., Jansen, R., Liu, Y.*, et al.* (2002). Subcellular localization of the yeast proteome. Genes Dev. *16*, 707-719.

Lee, P.R., Song, S., Ro, H.S., Park, C.J., Lippincott, J., Li, R., Pringle, J.R., De Virgilio, C., Longtine, M.S., and Lee, K.S. (2002). Bni5p, a septin-interacting protein, is required for normal septin function and cytokinesis in *Saccharomyces cerevisiae*. Mol. Cell. Biol. *22*, 6906-6920.

Magliery, T.J., Wilson, C.G., Pan, W., Mishler, D., Ghosh, I., Hamilton, A.D., and Regan, L. (2005). Detecting protein-protein interactions with a green fluorescent protein fragment reassembly trap: scope and mechanism. J. Am. Chem. Soc. *127*, 146-157.

Malicki, J., and Avidor-Reiss, T. (2014). From the cytoplasm into the cilium: bon voyage. Organogenesis *10*, 138-157.

McMurray, M.A., Bertin, A., Garcia, G., 3rd, Lam, L., Nogales, E., and Thorner, J. (2011). Septin filament formation is essential in budding yeast. Dev. Cell *20*, 540-549.

McMurray, M.A., and Thorner, J. (2009). Septins: molecular partitioning and the generation of cellular asymmetry. Cell Div. *4*, 18.

Meitinger, F., Boehm, M.E., Hofmann, A., Hub, B., Zentgraf, H., Lehmann, W.D., and Pereira, G. (2011). Phosphorylation-dependent regulation of the F-BAR protein Hof1 during cytokinesis. Genes Dev. *25*, 875-888.

Meitinger, F., Palani, S., Hub, B., and Pereira, G. (2013). Dual function of the NDR-kinase Dbf2

in the regulation of the F-BAR protein Hof1 during cytokinesis. Mol. Biol. Cell *24*, 1290-1304.

Miller, K.E., Kim, Y., Huh, W.K., and Park, H.O. (2015). Bimolecular fluorescence complementation (BiFC) analysis: advances and recent applications for genome-wide interaction studies. J. Mol. Biol. *427*, 2039-2055.

Millson, S., Truman, A.W., King, V., Prodromou, C., Pearl, L.H., and Piper, P.W. (2005). A two-hybrid screen of the yeast proteome for Hsp90 interactors uncovers a novel Hsp90 chaperone requirement in the activity of a stress-activated mitogen-activated protein kinase, Slt2p (Mpk1p). Eukaryot. Cell *4*, 849-860.

Mino, A., Tanaka, K., Kamei, T., Umikawa, M., Fujiwara, T., and Takai, Y. (1998). Shs1p: a novel member of septin that interacts with Spa2p, involved in polarized growth in *Saccharomyces cerevisiae*. Biochem. Biophys. Res. Commun. *251*, 732-736.

Mostowy, S., and Cossart, P. (2012). Septins: the fourth component of the cytoskeleton. Nat. Rev. Mol. Cell Biol*. 13*, 183-194.

Nagaraj, S., Rajendran, A., Jackson, C.E., and Longtine, M.S. (2008). Role of nucleotide binding in septin-septin interactions and septin localization in *Saccharomyces cerevisiae*. Mol. Cell. Biol. *28*, 5120-5137.

Nishihama, R., Schreiter, J.H., Onishi, M., Vallen, E.A., Hanna, J., Moravcevic, K., Lippincott , M.F., Han, H., Lemmon, M.A., Pringle, J.R.*, et al.* (2009). Role of Inn1 and its interactions with Hof1 and Cyk3 in promoting cleavage furrow and septum formation in *S. cerevisiae*. J. Cell Biol. *185*, 995-1012.

Oh, Y., and Bi, E. (2011). Septin structure and function in yeast and beyond. Trends Cell Biol. *21*, 141-148.

Oh, Y., Schreiter, J., Nishihama, R., Wloka, C., and Bi, E. (2013). Targeting and functional mechanisms of the cytokinesis-related F-BAR protein Hof1 during the cell cycle. Mol. Biol. Cell *24*, 1305-1320.

Ohashi, K., and Mizuno, K. (2014). A novel pair of split Venus fragments to detect protein-protein interactions by *in vitro* and *in vivo* bimolecular fluorescence complementation assays. Methods Mol. Biol. *1174*, 247-262.

Ong, K., Wloka, C., Okada, S., Svitkina, T., and Bi, E. (2014). Architecture and dynamic remodelling of the septin cytoskeleton during the cell cycle. Nature Commun. *5*, 5698.

Padilla-Parra, S., and Tramier, M. (2012). FRET microscopy in the living cell: different approaches, strengths and weaknesses. Bioessays *34*, 369-376.

Patasi, C., Godocikova, J., Michlikova, S., Nie, Y., Kacerikova, R., Kvalova, K., Raunser, S., and Farkasovsky, M. (2015). The role of Bni5 in the regulation of septin higher-order structure

formation. Biol. Chem. *396*, 1325-1337.

Remy, I., and Michnick, S.W. (2015). Mapping biochemical networks with protein fragment complementation assays. Methods Mol. Biol. *1278*, 467-481.

Renz, C., Oeljeklaus, S., Grinhagens, S., Warscheid, B., Johnsson, N., and Gronemeyer, T. (2016). Identification of cell cycle-dependent interaction partners of the septins by quantitative mass spectrometry. PloS One *11*, e0148340.

Rodal, A.A., Kozubowski, L., Goode, B.L., Drubin, D.G., and Hartwig, J.H. (2005). Actin and septin ultrastructures at the budding yeast cell cortex. Mol. Biol. Cell *16*, 372-384.

Saarikangas, J., and Barral, Y. (2011). The emerging functions of septins in metazoans. EMBO Rep. *12*, 1118-1126.

Sambrook, J., and Russell, D.W. (2001). Molecular Cloning: A Laboratory Manual, 3rd ed. (Cold Spring Harbor, NY: Cold Spring Harbor Laboratory Press).

Schneider, C., Grois, J., Renz, C., Gronemeyer, T., and Johnsson, N. (2013). Septin rings act as a template for myosin higher-order structures and inhibit redundant polarity establishment. J. Cell Sci. *126*, 3390-3400.

Shulewitz, M.J., Inouye, C.J., and Thorner, J. (1999). Hsl7 localizes to a septin ring and serves as an adapter in a regulatory pathway that relieves tyrosine phosphorylation of Cdc28 protein kinase in *Saccharomyces cerevisiae*. Mol. Cell. Biol. *19*, 7123-7137.

Sikorski, R.S., and Hieter, P. (1989). A system of shuttle vectors and yeast host strains designed for efficient manipulation of DNA in *Saccharomyces cerevisiae*. Genetics *122*, 19-27.

Toure, A., Rode, B., Hunnicutt, G.R., Escalier, D., and Gacon, G. (2011). Septins at the annulus of mammalian sperm. Biol. Chem. *392*, 799-803.

Versele, M., Gullbrand, B., Shulewitz, M.J., Cid, V.J., Bahmanyar, S., Chen, R.E., Barth, P., Alber, T., and Thorner, J. (2004). Protein-protein interactions governing septin heteropentamer assembly and septin filament organization in *Saccharomyces cerevisiae*. Mol. Biol. Cell *15*, 4568-4583.

Versele, M., and Thorner, J. (2004). Septin collar formation in budding yeast requires GTP binding and direct phosphorylation by the PAK, Cla4. J. Cell Biol. *164*, 701-715.

Wloka, C., and Bi, E. (2012). Mechanisms of cytokinesis in budding yeast. Cytoskeleton *69*, 710-726.

Wu, H., Guo, J., Zhou, Y.T., and Gao, X.D. (2015). The anillin-related region of Bud4 is the major functional determinant for Bud4's function in septin organization during bud growth and axial bud site selection in budding yeast. Eukaryot. Cell *14*, 241-251.

Table 1. Yeast strains used in this study.

Strain	Genotype	Reference
BY4741	*MAT**a** leu2Δ ura3Δ met15Δ his3Δ*	(Brachmann et al., 1998)
BY4742	*MATα leu2Δ ura3Δ met15Δ his3Δ*	(Brachmann et al., 1998)
GFY-42	BY4741; *cdc10Δ::CDC10::mCherry::ADH1(t)::SpHIS5*	(Finnigan et al., 2015b)
GFY-59[1]	BY4741; *cdc11Δ::CDC11::mCherry::ADH1(t)::SpHIS5*	This study
GFY-1794[2]	BY4742; *cdc10Δ::GFPβ10::Linker(32)::CDC10::ADH1(t)::Hyg^R cdc11Δ::CDC11::mCherry::SpHIS5*	This study
GFY-1570[3]	BY4741; *cdc10Δ::CDC10::Linker(33)::GFPβ11::ADH1(t)::Nat^R*	This study
GFY-1979[4]	BY4741; *PGK1::Linker(33)::GFPβ11::ADH1(t)::Kan^R*	This study
GFY-1983[5]	BY4741; *HSP82::Linker(33)::GFPβ11::ADH1(t)::Kan^R*	This study
GFY-2035[6]	BY4741; *CDC19::Linker(43)::GFPβ11::SHS1(t)::Kan^R*	This study
GFY-2036[6]	BY4741; *GPP1::Linker(43)::GFPβ11::SHS1(t)::Kan^R*	This study
GFY-2043[6]	BY4741; *TPI1::Linker(43)::GFPβ11::SHS1(t)::Kan^R*	This study
GFY-1793[7]	BY4742; *cdc3Δ::GFPβ10::Linker(18)::CDC3::ADH1(t)::Hyg^R cdc10Δ::CDC10::mCherry::SpHIS5*	This study
GFY-1851[8]	BY4741; *cdc10Δ::CDC10::GFPβ11::ADH1(t)::Hyg^R*	This study
GFY-1801[9]	BY4742; *cdc10Δ::GFPβ10::Linker(5)::CDC10::ADH1(t)::Hyg^R cdc11Δ::CDC11::mCherry::SpHIS5*	This study
GFY-1798	BY4742; *cdc3Δ::GFPβ10::Linker(5)::CDC3::ADH1(t)::Hyg^R cdc10Δ::CDC10::mCherry::SpHIS5*	This study
GFY-1803	BY4742; *cdc12Δ::GFPβ10::Linker(5)::CDC12::ADH1(t)::Hyg^R*	This study

	cdc10Δ::CDC10::mCherry::SpHIS5	
GFY-1804	BY4742; *cdc11Δ::GFPβ10::Linker(5)::CDC11::ADH1(t)::Hyg^R* *cdc10Δ::CDC10::mCherry::SpHIS5*	This study
GFY-1807	BY4742; *shs1Δ::GFPβ10::Linker(5)::SHS1::ADH1(t)::Hyg^R* *cdc10Δ::CDC10::mCherry::SpHIS5*	This study
GFY-1796	BY4742; *cdc10Δ::GFPβ10::Linker(18)::CDC10::ADH1(t)::Hyg^R* *cdc11Δ::CDC11::mCherry::SpHIS5*	This study
GFY-1793	BY4742; *cdc3Δ::GFPβ10::Linker(18)::CDC3::ADH1(t)::Hyg^R* *cdc10Δ::CDC10::mCherry::SpHIS5*	This study
GFY-1797	BY4742; *cdc12Δ::GFPβ10::Linker(18)::CDC12::ADH1(t)::Hyg^R* *cdc10Δ::CDC10::mCherry::SpHIS5*	This study
GFY-1795[10]	BY4742; *cdc11Δ::GFPβ10::Linker(18)::CDC11::ADH1(t)::Hyg^R* *cdc10Δ::CDC10::mCherry::SpHIS5*	This study
GFY-1806	BY4742; *shs1Δ::GFPβ10::Linker(18)::SHS1::ADH1(t)::Hyg^R* *cdc10Δ::CDC10::mCherry::SpHIS5*	This study
GFY-1852[11]	BY4741; *cdc10Δ::CDC10::Linker(10)::GFPβ11::ADH1(t)::Hyg^R*	This study
GFY-1853[12]	BY4741; *cdc10Δ::CDC10::Linker(20)::GFPβ11::ADH1(t)::Hyg^R*	This study
GFY-1845	BY4741; *cdc3Δ::CDC3::GFPβ11::ADH1(t)::Hyg^R*	This study
GFY-1848	BY4741; *cdc12Δ::CDC12::GFPβ11::ADH1(t)::Hyg^R*	This study
GFY-1842	BY4741; *cdc11Δ::CDC11::GFPβ11::ADH1(t)::Hyg^R*	This study
GFY-1839	BY4741; *shs1Δ::SHS1::GFPβ11::ADH1(t)::Hyg^R*	This study
GFY-1809	BY4742; *bni5Δ::GFPβ10::Linker(18)::BNI5::ADH1(t)::Hyg^R* *cdc10Δ::CDC10::mCherry::SpHIS5*	This study
GFY-1572	BY4741; *cdc3Δ::CDC3::Linker(33)::GFPβ11::ADH1(t)::Nat^R*	This study
GFY-1571	BY4741; *cdc12Δ::CDC12::Linker(33)::GFPβ11::ADH1(t)::Nat^R*	This study

GFY-1573	BY4741; *cdc11Δ::CDC11::Linker(33)::GFPβ11::ADH1(t)::Nat^R*	This study
GFY-1567	BY4741; *shs1Δ::SHS1::Linker(33)::GFPβ11::ADH1(t)::Nat^R*	This study
GFY-1735	BY4741; *bni5Δ::BNI5::Linker(33)::GFPβ11::ADH1(t)::Nat^R*	This study
GFY-1899	BY4742; *nis1Δ::GFPβ10::Linker(18)::NIS1::ADH1(t)::Hyg^R cdc10Δ::CDC10::mCherry::SpHIS5*	This study
GFY-1854	BY4741; *nis1Δ::NIS1::Linker(33)::GFPβ11::ADH1(t)::Hyg^R*	This study
GFY-1992[13]	BY4742; *hsl1Δ::GFPβ10::Linker(32)::HSL1(1-1518)::ADH1(t)::Kan^R cdc10Δ::CDC10::mCherry::SpHIS5*	This study
GFY-1995[14]	BY4742; *hsl1Δ::GFPβ10::Linker(32)::HSL1(611-950 R635A R636A K645A H648A K649A R653A K654A K775A E776A N777A R828A L831A)::ADH1(t)::Kan^R cdc10Δ::CDC10::mCherry::SpHIS5*	This study
GFY-1997[15]	BY4742; *hsl1Δ::GFPβ10::Linker(32)::HSL1(611-950; 1245-1518 R635A R636A K645A H648A K649A R653A K654A K775A E776A N777A R828A L831A)::ADH1(t)::Kan^R cdc10Δ::CDC10::mCherry::SpHIS5*	This study
GFY-1846	BY4741; *cdc3Δ::CDC3::Linker(10)::GFPβ11::ADH1(t)::Hyg^R*	This study
GFY-1849	BY4741; *cdc12Δ::CDC12::Linker(10)::GFPβ11::ADH1(t)::Hyg^R*	This study
GFY-1843	BY4741; *cdc11Δ::CDC11::Linker(10)::GFPβ11::ADH1(t)::Hyg^R*	This study
GFY-1840	BY4741; *shs1Δ::SHS1::Linker(10)::GFPβ11::ADH1(t)::Hyg^R*	This study
GFY-1847	BY4741; *cdc3Δ::CDC3::Linker(20)::GFPβ11::ADH1(t)::Hyg^R*	This study
GFY-2044	BY4741; *cdc12Δ::CDC12::Linker(20)::GFPβ11::ADH1(t)::Hyg^R*	This study
GFY-1844	BY4741; *cdc11Δ::CDC11::Linker(20)::GFPβ11::ADH1(t)::Hyg^R*	This study
GFY-1841	BY4741; *shs1Δ::SHS1::Linker(20)::GFPβ11::ADH1(t)::Hyg^R*	This study
GFY-1996	BY4742; *hsl1Δ::GFPβ10::Linker(18)::HSL1(611-950; 1245-*	This study

	1518 R635A R636A K645A H648A K649A R653A K654A K775A E776A N777A R828A L831A)::ADH1(t)::Kan^R cdc10Δ::CDC10::mCherry::SpHIS5	
GFY-1998	BY4742; *hsl1Δ::GFPβ10::Linker(5)::HSL1(611-950; 1245-1518 R635A R636A K645A H648A K649A R653A K654A K775A E776A N777A R828A L831A)::ADH1(t)::Kan^R cdc10Δ::CDC10::mCherry::SpHIS5*	This study
GFY-1977[16]	BY4741; *PGK1::eGFP::ADH1(t)::Kan^R*	This study
GFY-1981[16]	BY4741; *HSP82::eGFP::ADH1(t)::Kan^R*	This study
GFY-2031[17]	BY4741; *TPI1::eGFP::ADH1(t)::Hyg^R*	This study
GFY-2033[17]	BY4741; *GPP1::eGFP::ADH1(t)::Hyg^R*	This study
GFY-2034[17]	BY4741; *CDC19::eGFP::ADH1(t)::Hyg^R*	This study
GFY-1318	BY4741; *CDC10::mCherry::Kan^R bni5Δ::GFP::BNI5::SpHIS5 cdc11Δ::CDC11::Hyg^R SHS1 + pJT1520*	(Finnigan et al., 2015a)

[1]Strain was constructed by integrating *CDC11::mCherry::ADH1(t)::SpHIS5* amplified from pGF-IVL1 into *cdc11Δ::Kan^R* yeast (GFY-150). The strain was selected twice on 5-FOA-containing medium to counter-select for the WT *CDC11*-expressing covering vector. Unless otherwise noted, all strains were selected on 5-FOA to remove these covering vector(s) prior to diploid formation.

[2]Strain was constructed by integrating the tagged *CDC10* allele (from pGF-IVL824) into *cdc10Δ* yeast (GFY-1603). The *GFPβ10* sequence is MDLPDDHYLSTQTILSKDLN (Cabantous et al., 2013). The 32-residue linker sequence is DVGGGGSEGGGSGGPGSGGEGSAGGGSAGGGS. *CDC11* was tagged with mCherry by amplifying the entire locus from chromosomal DNA from GFY-59 and transforming into GFY-1643. N-terminally tagged proteins were constructed using this strategy unless otherwise noted. All the flexible linker sequences (N- or C-terminal) were

modeled as previously described (Cabantous et al., 2013).

[3]Strain was constructed by integrating the tagged *CDC10* allele (from pGF-IVL810) into *cdc10*Δ yeast (GFY-140). The *GFPβ11* sequence is EKRDHMVLLEYVTAAGITDAS (Cabantous et al., 2013). The 33-residue linker is DYKDDDDKGSGAGGSPGGGSGGSGSSASGGSTS. C-terminally tagged strains were constructed using this strategy unless otherwise noted.

[4]Strain was constructed by creating an integrating vector containing the entire PGK1 ORF fused to the C-terminal tag including the drug cassette, and finally, 491 bps of 3' UTR (pGF-IVL1054). The entire cassette was amplified and transformed into BY4741 yeast.

[5]Strain was constructed by first creating an integrating vector containing 471 bps of the *HSP82* ORF fused to the C-terminal tag including the drug cassette, and finally, 500 bps of 3' UTR (pGF-IVL1056). The entire cassette was amplified and transformed into BY4741 yeast.

[6]These strains were constructed by amplifying the C-terminal cassette (from pGF-V763) including a slightly larger linker sequence (including an upstream GRRIPGLINP) with short 30 bp oligonucleotide tails to each locus of interest. 469 bps of *SHS1* 3' UTR sequence was used as the terminator, and the promoter of *CCW12* (992 bps) replaced the P_{tef} sequence of the MX cassette. Strains were confirmed via diagnostic PCR and DNA sequencing of the full junction of the gene with the C-terminal tag.

[7]The 18-residue linker sequence is DVGGGGSEGGGSGGPGSG.

[8]There is no linker between the C-terminus of *CDC10* and the *GFPβ11* sequence.

[9]The 5-residue linker has the sequence DVGGG.

[10]Strains with an N-terminal *GFPβ10* tag with a 32-residue linker appended to *CDC11* were lethal.

[11]The 10-residue linker has the sequence GSSASGGSTS.

[12]The 20-residue linker has the sequence GSPGGGSGGSGSSASGGSTS.

[13]The tagged *HSL1* construct was integrated into *hsl1*Δ*::Hyg*^{R} yeast (GFY-1902) by amplifying two PCR fragments that contained overlapping sequence within the *HSL1* ORF from plasmid

pGF-IVL1034.

[14]This Hsl1 construct has a putative NLS sequence mutated to Alanine to prevent nuclear import as well as the KEN (residues 775-781) and D-box (residues 828-836) destruction motifs to prevent APC-dependent degradation.

[15]This Hsl1 construct contains both the septin binding domain (residues 611-950) as well sequence containing the C-terminal KA1 domain (residues 1245-1518), both of which are required for optimal localization of Hsl1 to the septin collar *in vivo* (Finnigan et al., 2016).

[16]Strains were constructed similar to GFY-1979 and GFY-1983 using full-length eGFP and confirmed via DNA Sequencing.

[17]Strains were constructed similar to GFY-2035, using *eGFP::ADH1(t)::Hyg*^{R} as template DNA. Proper integration was confirmed via DNA sequencing.

Table 2. Plasmids used in this study

Plasmid	Description	Reference
pRS315	CEN; *LEU2 AMP*	(Sikorski and Hieter, 1989)
pRS316	CEN; *URA3 AMP*	(Sikorski and Hieter, 1989)
pGF-IVL794[1]	pRS315; *prGAL1/10::GFPβ1-9(A)::ADH1(t)::Kan^R*	This study
pGF-IVL795[2]	pRS315; *prGAL1/10::GFPβ1-9(B)::ADH1(t)::Kan^R*	This study
pGF-IVL553[3]	pRS315; *prNIS1::NIS1::ADH1(t)::Kan^R*	This study
pGF-IVL521	pRS315; *prCDC11::HSL1(1-1518)::eGFP::ADH1(t)::Kan^R*	(Finnigan et al., 2016)
pGF-IVL762[4]	pRS315; *prCDC11::hsl1(611-950 R635A R636A K645A H648A K649A R653A K654A)::eGFP::ADH(1)::Kan^R*	(Finnigan et al., 2016)
pGF-IVL536[5]	pRS315; *prCDC11::hsl1(611-950; 1245-1518)::eGFP::ADH1(t)::Kan^R*	(Finnigan et al., 2016)
pGF-IVL1095[6]	pRS315; *prBUD4::BUD4(623-774)::eGFP::ADH1(t)::Kan^R*	This study
pGF-IVL1110[7]	pRS315; *prHOF1:: eGFP::HOF1(293-355)::ADH1(t)::Kan^R*	This study
pGF-IVL1082	pRS315; *prBUD4::BUD4(623-774)::Linker(33)::GFPβ11::ADH1(t)::Kan^R*	This study
pGF-IVL1084	pRS315; *prHOF1::HOF1(293-355)::Linker(33)::GFPβ11::ADH1(t)::Kan^R*	This study
pGF-IVL1105	pRS316; *prGAL1/10::GFPβ1-9(A)::ADH1(t)::Kan^R*	This study

[1]The evolved *GFPβ1-9* was synthesized as a custom gene using a yeast codon bias. The "A" version designates the position of the last residue: this version ends with the sequence GPVLLPDNGS (Cabantous et al., 2013).

[2]A second variant of the *GFPβ1-9* was created identical to the "A" version, but ending with the sequence GPVLLP. The *prGAL1/10* promoter includes 814 bps of 5' UTR sequence.

[3]The endogenous *NIS1* promoter includes 576 bps of 5' UTR sequence.

[4]The putative NLS signal within the N-terminus of Hsl1(611-950) was experimentally determined to require residues *R635 R636 K645 H648 K649 R653 K654* for constructs beginning at residue 611 (Finnigan et al., 2016). Mutation of these residues to Alanine eliminates nuclear localization of this Hsl1 fragment.

[5]The combination of the central Hsl1(611-950) septin binding domain and the C-terminal KA1 domain contained within Hsl1(1245-1518) has been shown to be sufficient to efficiently target Hsl1 to the bud neck *in vivo* (Finnigan et al., 2016).

[6]The Bud4(623-774) fragment has been previously shown to be sufficient to target to the septin collar *in vivo* (Wu et al., 2015). The *BUD4* sequence was amplified from pGF-V416 and assembled by *in vivo* ligation and homologous recombination. Both N- and C-terminal eGFP fusions to this Bud4 fragment displayed localization to the septin collar.

[7]The Hof1(293-355) fragment has been previously shown to be sufficient to target to the septin collar *in vivo* (Meitinger et al., 2013). The *HOF1* sequence was amplified from pGF-V454 and assembled via *in vivo* ligation. Only the N-terminal eGFP fusion to this Hof1 fragment displayed localization to the septin collar (data not shown).

FIGURE LEGENDS

Figure 1. Implementation of the tripartite split-GFP system in live yeast. (A) A mating-based strategy to generate cells expressing all of the components of the tripartite split-GFP method. A haploid that expresses an N-terminally β10-tagged protein of interest from its endogenous promoter at its native chromosomal locus (and also expresses an independent marker for the subcellular location of interest, where available) is mated to a haploid of opposite mating type that expresses a C-terminally β11-tagged protein of interest from its endogenous promoter at its native chromosomal locus and also harbors a *CEN* plasmid that expresses from a regulatable promoter the GFPβ1-9 barrel. (B) All three components of the tripartite split-GFP system are required to generate a protein-protein interaction signal *in vivo*. Diploids strains (1-8; Table S3) that express all three or only two, one, or no components of the tripartite split-GFP system, as indicated, were constructed as in (A) by two rounds of selection on minimal (S)-Leu-His medium with 2% glucose. GFPβ1-9 was carried on a *LEU2*-marked *CEN* plasmid (pGF-IVL794) and expressed under control of the *GAL1/10* promoter. Cultures of the indicated diploids were grown overnight to saturation in S-Leu-His medium with 2% raffinose-0.2% sucrose, back-diluted into the same medium with 2% galactose, grown at 30°C for 4.5 h, harvested, washed, and imaged by fluorescence microscopy. All images were captured after the identical exposure time and processed using ImageJ. Dotted white line, cell periphery. Scale bar, 2 μm. E.V., empty vector (pRS315). Diploid 1 contained one copy of β10-(32-residue linker)-Cdc10 and one copy of Cdc10-(33-residue linker)-β11 (see Fig. S1). (C) Quantification of the average GFP fluorescence at the bud neck in budded cells (25-100 per culture) for the strains in (B). Error bar, S.E.M. Dotted red line, average intrinsic background fluorescence (~35-40 pixels) at the bud neck in cells lacking the components of the tripartite split-GFP system for images taken at the identical exposure time. (D) *Left*, confirmation that the five proteins indicated are abundant cytosolic proteins. Strains expressing each of the indicated proteins (see Table S4) as an eGFP fusion (GFY-1977, GFY-1981, GFY-2034, GFY-2030 and GFY-2033) were grown to saturation in rich

(YPD) medium, back-diluted into fresh YPD, grown to mid-exponential phase, and imaged as in (A), except that the exposure times varied: Gpp1-eGFP (150 ms); Hsp82-eGFP (150 ms); Cdc19-eGFP (100 ms); Pgk1-eGFP (50 ms); and Tpi1-eGFP (50 ms). *Right*, none of five extremely abundant cytosolic proteins exhibits more than a very weak interaction with any septin. Representative examples for the interaction of the indicated β11-tagged proteins with β10-Cdc3 using the tripartite split-GFP method. In diploids 164, 170, 272, 282 and 277 expressing the indicated proteins, expression of GFPβ1-9 was induced and the cells imaged as in (B). (E) Quantification, as in (C), of the fluorescent signal at the bud neck in dividing diploids (25-100 per culture) that expressed each abundant β11-tagged cytosolic protein with each β10-septin (see Table S3 for complete list).

Figure 2. Influence of linker length on the output of the tripartite split-GFP system. (A) *Left*, diploid yeast (strains 24-28) were generated that express Cdc10-β11 along with each of the β10-septins (with the tags appended using the linker lengths given), as indicated, as well as a *CEN* plasmid (pGF-IVL794) to express GFPβ1-9 (not shown). *Right*, cultures of each of the corresponding diploids were grown and the cells imaged as in Fig. 1B. Representative images are shown and the percentage of the cells displaying the pattern shown is indicated in the upper righthand corner. The fiducial marker for the septin collar is Cdc10-mCh expressed in the same cells, except in the cells expressing Cdc10-β11 and β10-Cdc10 (*top panel*), where the marker is Cdc11-mCh. (B) Heat map depicting the percentage of cells (number in the box) in the population exhibiting a readily detectable green fluorescent signal for 40 diploids (strains 10-14, 17-21, 24-28, 31-35, 38-42, 45-49, 52-56, and 59-63), with the arrangements shown in (A), but where the linker connecting the β11 tag to the C-terminus of Cdc10 was systematically varied from 0 to 10, 20, or 33 residues, as indicated (*at top*), and where the linker between the N-terminal β10 tag and the N terminus of each septin was either 5 or 18 residues, as indicated (*to the left*). (C) Quantification, as in Fig. 1C, of the data for the diploids where the linker lengths for

Cdc10-β11 were 0, 10, 20 or 33 residues, as indicated, and the linker between the N-terminal β10 tag and the N terminus of each septin was 5 residues (strains 10-14, 17-21, 24-28, and 21-35).

Figure 3. Further analysis of septin-septin interactions using the tripartite split-GFP system. Each of the essential septins (Cdc3, Cdc10, Cdc11 and Cdc12) was tagged with an N-terminal β10 tag and a 5-residue linker and then combined by mating, as in Fig. 1A, with each of the five mitotic septins tagged at their immediate C-terminal end with β11, as indicated schematically in the left-hand diagrams in each panel. Except in the cases where both copies of the same septin were tagged (*e.g.*, β10-Cdc10 and Cdc10-β11), a second (WT) copy of each tagged subunit is present, but has been omitted from the diagram for clarity. The resulting diploids were grown, induced with galactose, washed and imaged as in Fig. 1B. (A) Diploids 73-77; (B) Diploids 66-70; (C) Diploids 101-105; and (D) Diploid strains 80-84. For β10-Shs1 examined in the same way, see Fig. S4. The fiducial marker for the septin collar was Cdc10-mCh expressed in the same cells, except in the cells expressing β10-Cdc10 and Cdc10-β11, where the marker was Cdc11-mCh. (E) Quantification, as in Fig. 1C, of the data shown in panels A, B, C and D.

Figure 4. Interaction of Bni5 with the septin collar. (A) Cells (strain GFY-1318) expressing an eGFP-Bni5 fusion and co-expressing Cdc10-mCh were grown to mid-exponential phase and visualized by fluorescence microscopy. Representative cells with a medium-to-large bud and an intact septin collar prior to cytokinesis (*top panel*s) or with a split septin collar diagnostic of cells in cytokinesis (*bottom panels*) are shown. Dotted white line, cell periphery; scale bar, 2 μm. (B) Diploids (127, 120, 141, 134 and 148) expressing Bni5-$(linker)_{33}$-β11 and N-terminally β10-$(linker)_{18}$-tagged versions of the five mitotic septins (*left*) were visualized by fluorescence microscopy as in Fig 1B (*right*). For the strain expressing β10-$(linker)_{18}$-Cdc10 (*top panel*), the fiducial mark for the septin collar was Cdc11-mCh and, for all the others, Cdc10-mCh. (C) Quantification, as in Fig. 1C, of the data shown in panel B. (D) Diploids (151, 150, 153, 152 and

154) expressing β10-(linker)$_{18}$-Bni5 and C-terminally -(linker)$_{33}$-β11 tagged versions of the five mitotic septins (*left*) were visualized by fluorescence microscopy as in Fig 1B (*right*). *Bottom panels*, homotypic Bni5 interaction was assessed by examining a diploid (155) co-expressing Bni5-(linker)$_{33}$-β11 and β10-(linker)$_{18}$-Bni5. (E) Quantification, as in Fig. 1C, of the data shown in panel D.

Figure 5. Septin-binding domain of checkpoint kinase Hsl1 associates preferentially with Cdc3 and Cdc12. (A) Cells (strain GFY-42) expressing Cdc10-mCh and co-expressing from *CEN* plasmids, as indicated, either (*1*) full-length Hsl1-eGFP (pGF-IVL521), or (*2*) its septin-binding domain (residues 611-950) with a cryptic NLS mutated to alanine (Finnigan et al., 2016) (pGF-IVL762), or (*3*) its septin-binding domain (611-950) fused to its C-terminal PtdSer-binding KA1 domain (residues 1245-1518) (Finnigan et al., 2016) (pGF-IVL536), each with eGFP fused to its C-terminus, were grown and visualized by fluorescence microscopy as in Fig. 4A. Only cells with an intact septin collar were scored because, upon the onset of anaphase and formation of the split collar, Hsl1 is degraded (Burton and Solomon, 2000, 2001). (B) Diploids (176-190) expressing each of the three Hsl1 constructs in (A) N-terminally β10-(linker)$_{32}$-tagged and each of the five mitotic septins C-terminally -(linker)$_{33}$-β11 tagged (*left*) were visualized by fluorescence microscopy as in Fig 1B (*right*). For the 611-950 domain constructs (*2* and *3*) in these experiments, the cryptic NLS was mutated (R635A R636A K645A H648A K649A R653A K654A), as well as both the KEN (K775A E776A N777A) and D-box (R828A L831A) degradation motifs. (C) Quantification, as in Fig. 1C, of the data shown in panel B, except that only budded cells with an intact septin collar (i.e., that had not entered cytokinesis) were scored. (D) Sixty diploids (186-190, 206-235, and 247-271) were generated in which the linker lengths in both the β10-tagged 611-950;1245-1518 fragment and in the septin-β11 constructs were systematically shortened, as indicated, visualized by fluorescence microscopy as in Fig 1B, and quantified as in Fig. 1C. *Dotted green line*, best fit trend line for the Cdc3 and Cdc12 data

points; *dotted blue line*, best fit trend line for Cdc10 data points.

Figure 6. Bud neck-localized protein Nis1 does not interact directly with septins. (A) Cells (strain GFY-42) expressing Cdc10-mCh and co-expressing Nis1-eGFP under the control of its endogenous promoter from a *CEN* plasmid (pGF-IVL553) were grown and visualized as in Fig. 4A. *Upper panel*, GFP signal *(white triangles*) adjacent to the septin collar in budded cells prior to cytokinesis. *Bottom panel*, during cytokinesis, Nis1-eGFP localizes between the two rings generated by splitting of the septin collar. *Inset*, enlarged view of the merged image; scale bar, 1 μm. (B) Diploids (128, 121, 142, 135, and 149) expressing Nis1-$(linker)_{33}$-β11 and the β10-$(linker)_{18}$-tagged versions of each of the five mitotic septins (*left*), as well as either Cdc10-mCh or Cdc11-mCh (as indicated), were visualized as in Fig 1B (*right*). (C) Quantification, as in Fig. 1C, of the data shown in panel B. (D) Diploids (157-161, and 163) expressing β10-$(linker)_{18}$-Nis1 and C-terminally -$(linker)_{33}$-β11 tagged versions of each of the five mitotic septins (*left*), as well as Cdc10-mCh, were visualized as in Fig 1B (*right*). (E) Quantification, as in Fig. 1C, of the data shown in panel D.

Figure 7. Septin-binding domains of Bud4 and Hof1 have distinct subunit preferences. (A) Cells (strain GFY-42) expressing Cdc10-mCh and co-expressing Bud4(623-774)-eGFP under the control of the *BUD4* promoter from a *CEN* plasmid (pGF-IVL1095) were grown and visualized as in Fig. 4A. (B) Diploids (287-291) expressing Bud4(623-774)-$(linker)_{33}$-β11 from its native promoter on a *LEU2*-marked *CEN* plasmid (pGF-IVL1082), the β10-$(linker)_{18}$-tagged versions of each of the five mitotic septins (*left*), a *URA3*-marked *CEN* plasmid (pGF-IVL1005) expressing GFPβ1-9 from the *GAL1/GAL10* promoter (*not shown*), as well as either Cdc10-mCh or Cdc11-mCh (as indicated), were selected on SD-Ura-Leu medium, grown, induced with galactose, washed and imaged as in Fig. 1B. (C) Quantification, as in Fig. 1C, of the data shown in panel B. (D) Cells (strain GFY-42) expressing Cdc10-mCh and co-expressing eGFP-Hof1(293-355) under the control of the *HOF1* promoter from a *CEN* plasmid (pGF-IVL1110) were grown and

visualized as in Fig. 4A. (E) Diploids (292-296) expressing Hof1(293-355)-(linker)$_{33}$-β11 from its native promoter on a *LEU2*-marked *CEN* plasmid (pGF-IVL1082), the β10-(linker)$_{18}$-tagged versions of each of the five mitotic septins (*left*), a *URA3*-marked *CEN* plasmid (pGF-IVL1005) expressing GFPβ1-9 from the *GAL1/GAL10* promoter (*not shown*), as well as either Cdc10-mCh or Cdc11-mCh (as indicated), were treated and examined as in panel B. (F) Quantification, as in Fig. 1C, of the data shown in panel E.

Figure 8. Diagrammatic summary of the interactions of bud neck-localized proteins with specific septin subunits detected using the tripartite split-GFP assay. The linear hetero-octamer is depicted as it resides in paired filaments (conjoined via formation of cross-filament coiled coils between the CTEs on Cdc3 and Cdc12). The N terminal face of each septin is predicted to project 180° away from its CTE, based on the recently determined crystal structure of *S. cerevisiae* Cdc11 as a representative subunit (Brausemann et al., 2016). The C-terminus of Bni5 exhibited preferential interaction with the N terminal faces of Cdc11 and Shs1 (*thick red arrows*), whereas the N terminus of Bni5 was able to interact weakly with the C-termini of all five septins (*dotted red arrows*). The N terminus of the septin-binding domain of Hsl1 displayed preferential interaction with the C-termini of Cdc12 and Cdc3, whereas the C-terminus of the same fragment did not display a detectable interaction with any subunit. The C-terminus of the septin-binding domain of Bud4 exhibited preferential interaction with the N-termini of Cdc11 and /Shs1 and, weakly, Cdc3 (most likely due to the extremely long N-terminal extension on Cdc3), whereas the N-terminus of the same fragment did not display detectable interaction with any subunit. The C-terminus of the septin-binding domain of Hof1 displayed preferential interaction with the N-termini of Cdc10 and Cdc12 and, weakly Cdc3, whereas the N-terminus of the same fragment did not display detectable interaction with any subunit.

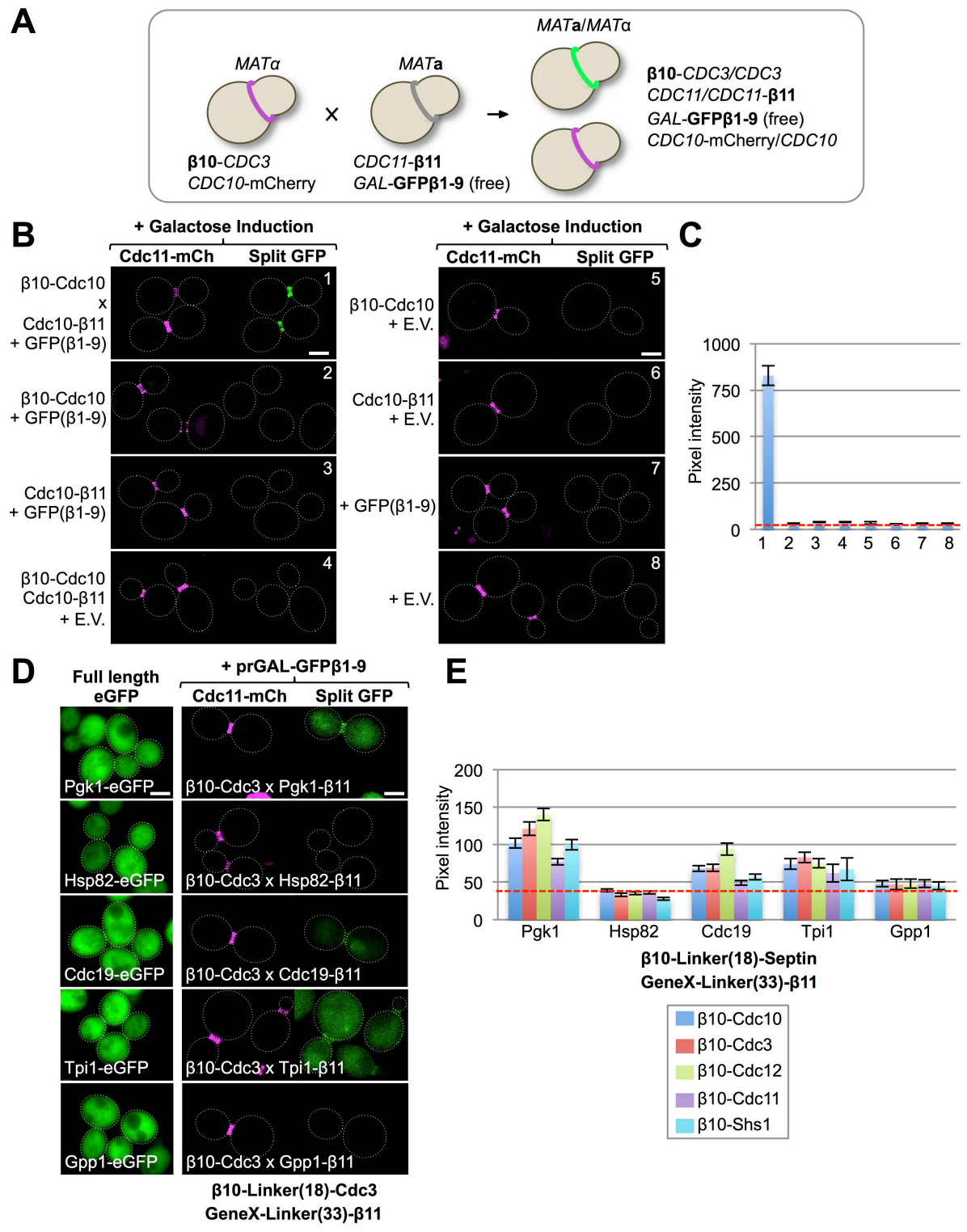
A
MATα
MATa
MATa/MATα
β10-CDC3
CDC10-mCherry
CDC11-β11
GAL-GFPβ1-9 (free)
β10-CDC3/CDC3
CDC11/CDC11-β11
GAL-GFPβ1-9 (free)
CDC10-mCherry/CDC10
B
+ Galactose Induction
Cdc11-mCh
Split GFP
β10-Cdc10 x Cdc10-β11 + GFP(β1-9)
β10-Cdc10 + GFP(β1-9)
Cdc10-β11 + GFP(β1-9)
β10-Cdc10 Cdc10-β11 + E.V.
β10-Cdc10 + E.V.
Cdc10-β11 + E.V.
+ GFP(β1-9)
+ E.V.
C
Pixel intensity
D
Full length eGFP
+ prGAL-GFPβ1-9
Pgk1-eGFP
Hsp82-eGFP
Cdc19-eGFP
Tpi1-eGFP
Gpp1-eGFP
β10-Cdc3 x Pgk1-β11
β10-Cdc3 x Hsp82-β11
β10-Cdc3 x Cdc19-β11
β10-Cdc3 x Tpi1-β11
β10-Cdc3 x Gpp1-β11
β10-Linker(18)-Cdc3
GeneX-Linker(33)-β11
E
Pixel intensity
Pgk1
Hsp82
Cdc19
Tpi1
Gpp1
β10-Linker(18)-Septin
GeneX-Linker(33)-β11
β10-Cdc10
β10-Cdc3
β10-Cdc12
β10-Cdc11
β10-Shs1

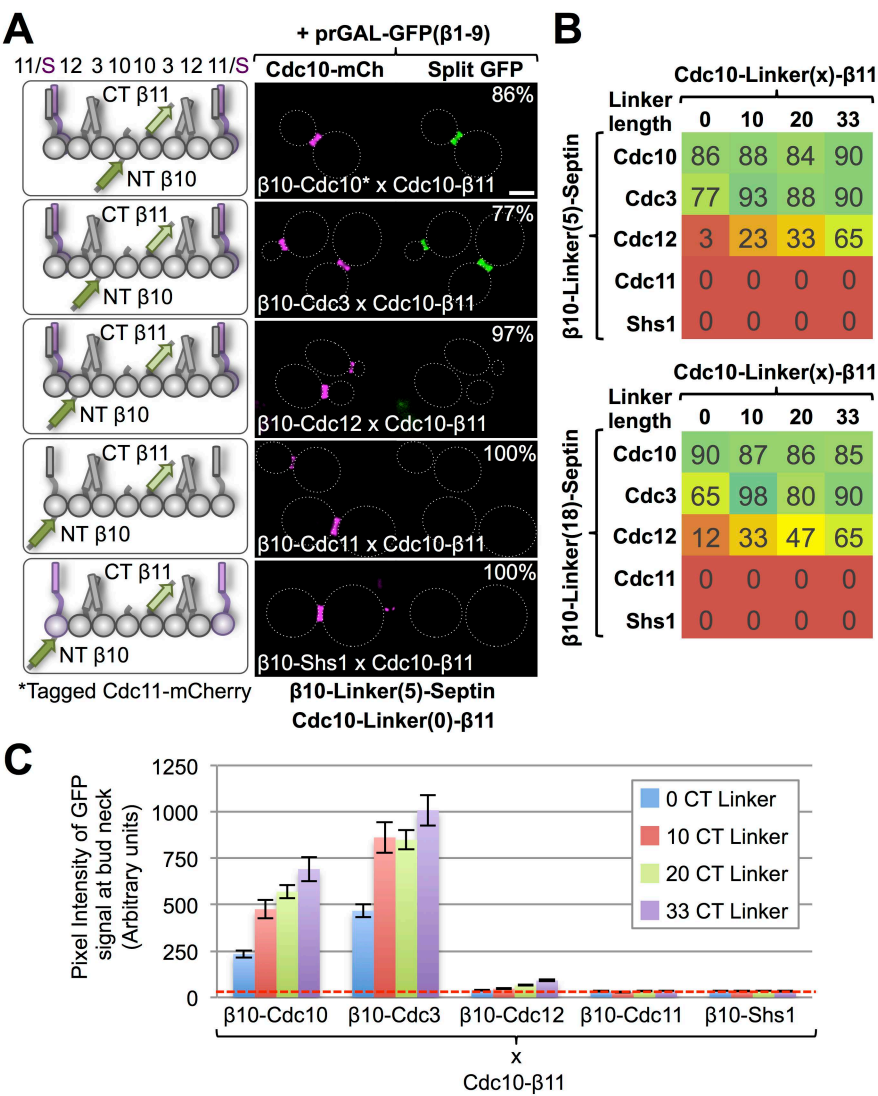
A
+ prGAL-GFP(β1-9)
11/S 12 3 10 10 3 12 11/S
Cdc10-mCh
Split GFP
CT β11
NT β10
86%
β10-Cdc10* x Cdc10-β11
77%
β10-Cdc3 x Cdc10-β11
97%
β10-Cdc12 x Cdc10-β11
100%
β10-Cdc11 x Cdc10-β11
100%
β10-Shs1 x Cdc10-β11
*Tagged Cdc11-mCherry
β10-Linker(5)-Septin
Cdc10-Linker(0)-β11
B
Cdc10-Linker(x)-β11
Linker length
0 10 20 33
β10-Linker(5)-Septin
Cdc10 86 88 84 90
Cdc3 77 93 88 90
Cdc12 3 23 33 65
Cdc11 0 0 0 0
Shs1 0 0 0 0
Cdc10-Linker(x)-β11
Linker length
0 10 20 33
β10-Linker(18)-Septin
Cdc10 90 87 86 85
Cdc3 65 98 80 90
Cdc12 12 33 47 65
Cdc11 0 0 0 0
Shs1 0 0 0 0
C
Pixel Intensity of GFP signal at bud neck (Arbitrary units)
1250
1000
750
500
250
0
0 CT Linker
10 CT Linker
20 CT Linker
33 CT Linker
β10-Cdc10
β10-Cdc3
β10-Cdc12
β10-Cdc11
β10-Shs1
x
Cdc10-β11

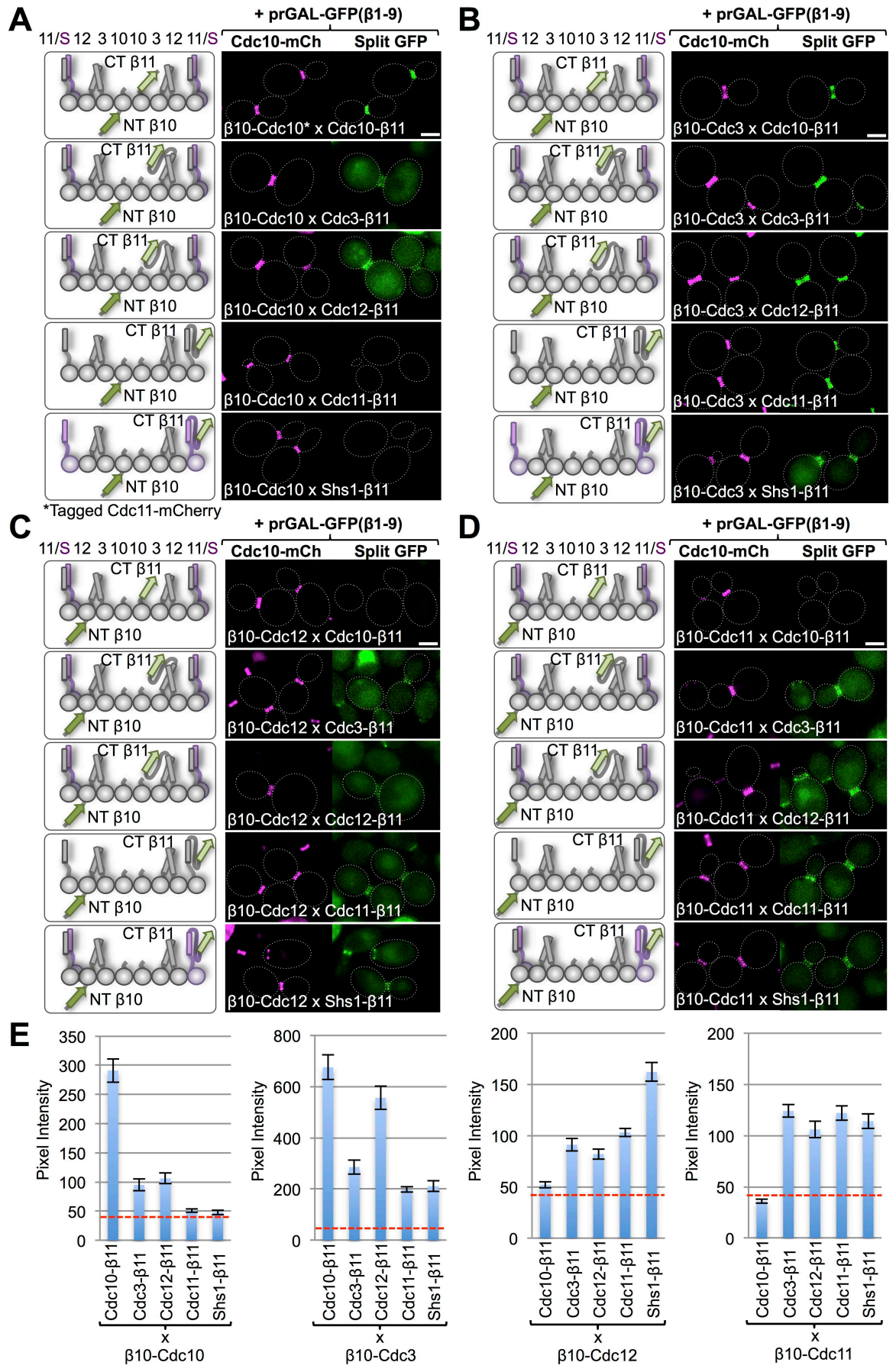
A
+ prGAL-GFP(β1-9)
11/S 12 3 10 10 3 12 11/S
Cdc10-mCh
Split GFP
CT β11
NT β10
β10-Cdc10* x Cdc10-β11
β10-Cdc10 x Cdc3-β11
β10-Cdc10 x Cdc12-β11
β10-Cdc10 x Cdc11-β11
β10-Cdc10 x Shs1-β11
*Tagged Cdc11-mCherry
B
β10-Cdc3 x Cdc10-β11
β10-Cdc3 x Cdc3-β11
β10-Cdc3 x Cdc12-β11
β10-Cdc3 x Cdc11-β11
β10-Cdc3 x Shs1-β11
C
β10-Cdc12 x Cdc10-β11
β10-Cdc12 x Cdc3-β11
β10-Cdc12 x Cdc12-β11
β10-Cdc12 x Cdc11-β11
β10-Cdc12 x Shs1-β11
D
β10-Cdc11 x Cdc10-β11
β10-Cdc11 x Cdc3-β11
β10-Cdc11 x Cdc12-β11
β10-Cdc11 x Cdc11-β11
β10-Cdc11 x Shs1-β11
E
Pixel Intensity
Cdc10-β11
Cdc3-β11
Cdc12-β11
Cdc11-β11
Shs1-β11
x
β10-Cdc10
β10-Cdc3
β10-Cdc12
β10-Cdc11

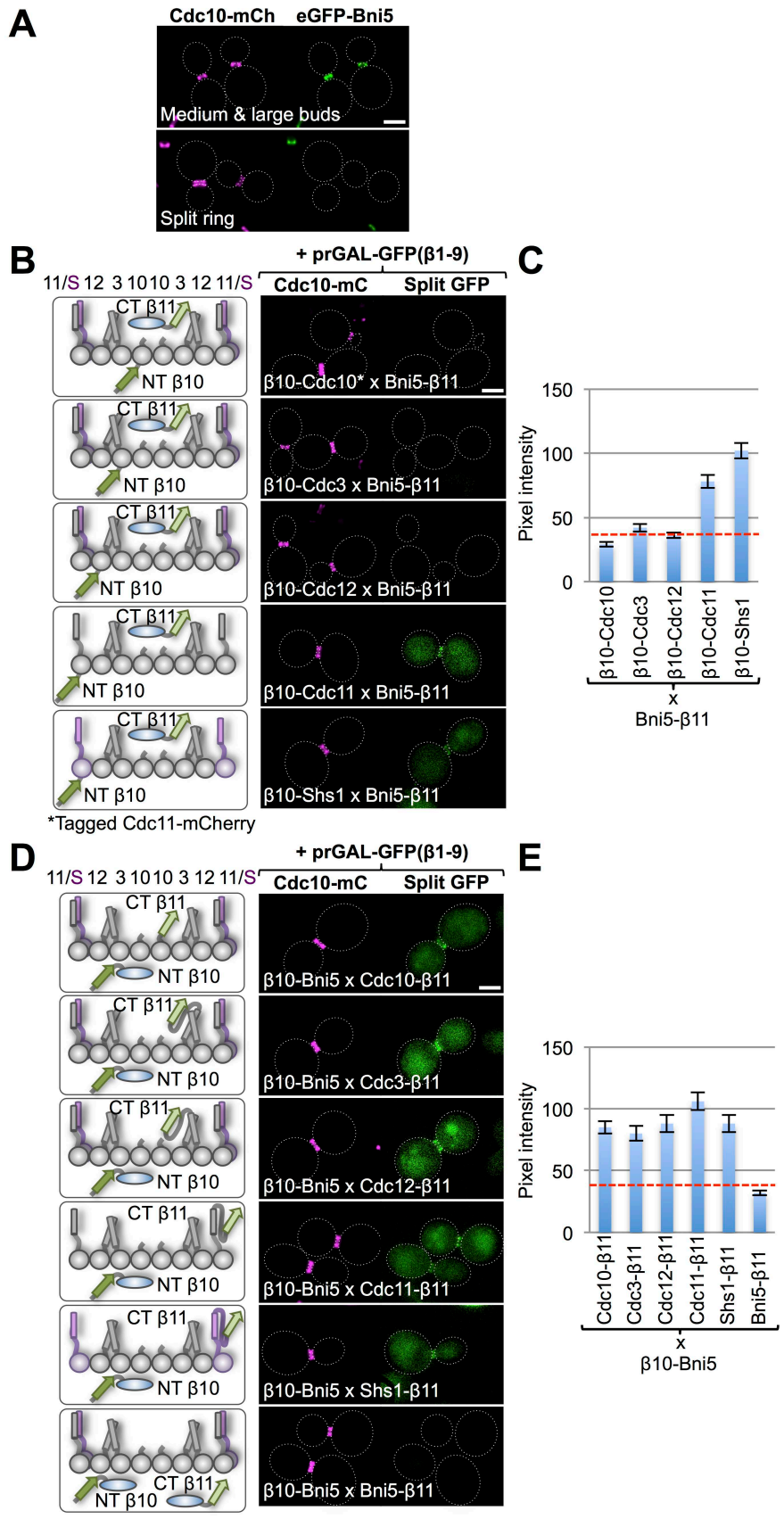
A
Cdc10-mCh
eGFP-Bni5
Medium & large buds
Split ring
B
+ prGAL-GFP(β1-9)
11/S 12 3 10 10 3 12 11/S
Cdc10-mC
Split GFP
CT β11
NT β10
β10-Cdc10* x Bni5-β11
β10-Cdc3 x Bni5-β11
β10-Cdc12 x Bni5-β11
β10-Cdc11 x Bni5-β11
β10-Shs1 x Bni5-β11
*Tagged Cdc11-mCherry
C
Pixel intensity
150
100
50
0
β10-Cdc10
β10-Cdc3
β10-Cdc12
β10-Cdc11
β10-Shs1
x
Bni5-β11
D
+ prGAL-GFP(β1-9)
11/S 12 3 10 10 3 12 11/S
Cdc10-mC
Split GFP
CT β11
NT β10
β10-Bni5 x Cdc10-β11
β10-Bni5 x Cdc3-β11
β10-Bni5 x Cdc12-β11
β10-Bni5 x Cdc11-β11
β10-Bni5 x Shs1-β11
β10-Bni5 x Bni5-β11
E
Pixel intensity
150
100
50
0
Cdc10-β11
Cdc3-β11
Cdc12-β11
Cdc11-β11
Shs1-β11
Bni5-β11
x
β10-Bni5

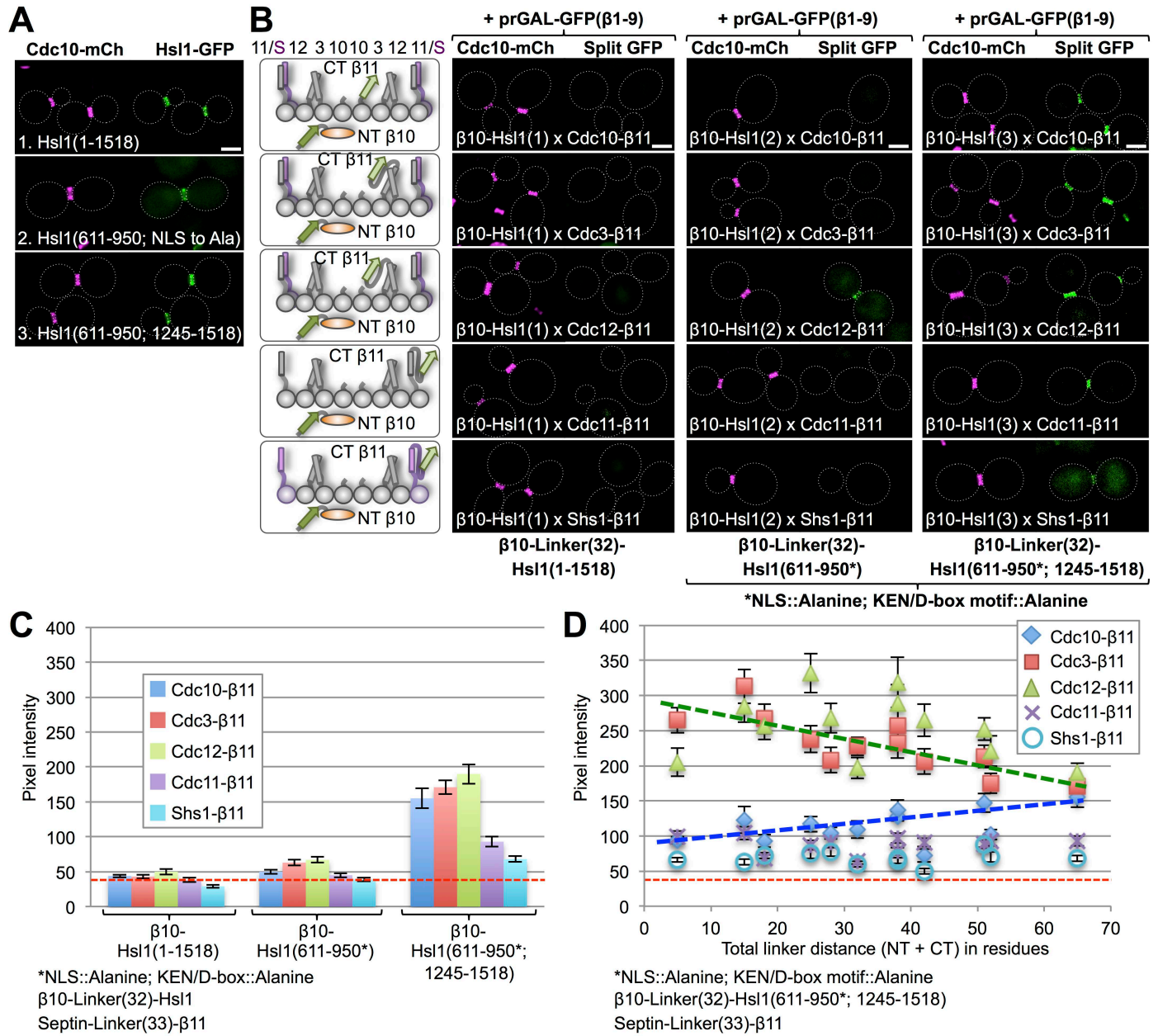
A
Cdc10-mCh
Hsl1-GFP
1. Hsl1(1-1518)
2. Hsl1(611-950; NLS to Ala)
3. Hsl1(611-950; 1245-1518)
B
11/S 12 3 10 10 3 12 11/S
CT β11
NT β10
+ prGAL-GFP(β1-9)
Cdc10-mCh
Split GFP
β10-Hsl1(1) x Cdc10-β11
β10-Hsl1(1) x Cdc3-β11
β10-Hsl1(1) x Cdc12-β11
β10-Hsl1(1) x Cdc11-β11
β10-Hsl1(1) x Shs1-β11
β10-Hsl1(2) x Cdc10-β11
β10-Hsl1(2) x Cdc3-β11
β10-Hsl1(2) x Cdc12-β11
β10-Hsl1(2) x Cdc11-β11
β10-Hsl1(2) x Shs1-β11
β10-Hsl1(3) x Cdc10-β11
β10-Hsl1(3) x Cdc3-β11
β10-Hsl1(3) x Cdc12-β11
β10-Hsl1(3) x Cdc11-β11
β10-Hsl1(3) x Shs1-β11
β10-Linker(32)-Hsl1(1-1518)
β10-Linker(32)-Hsl1(611-950*)
β10-Linker(32)-Hsl1(611-950*; 1245-1518)
*NLS::Alanine; KEN/D-box motif::Alanine
C
Pixel intensity
Cdc10-β11
Cdc3-β11
Cdc12-β11
Cdc11-β11
Shs1-β11
β10-Hsl1(1-1518)
β10-Hsl1(611-950*)
β10-Hsl1(611-950*; 1245-1518)
*NLS::Alanine; KEN/D-box::Alanine
β10-Linker(32)-Hsl1
Septin-Linker(33)-β11
D
Pixel intensity
Total linker distance (NT + CT) in residues
*NLS::Alanine; KEN/D-box motif::Alanine
β10-Linker(32)-Hsl1(611-950*; 1245-1518)
Septin-Linker(33)-β11

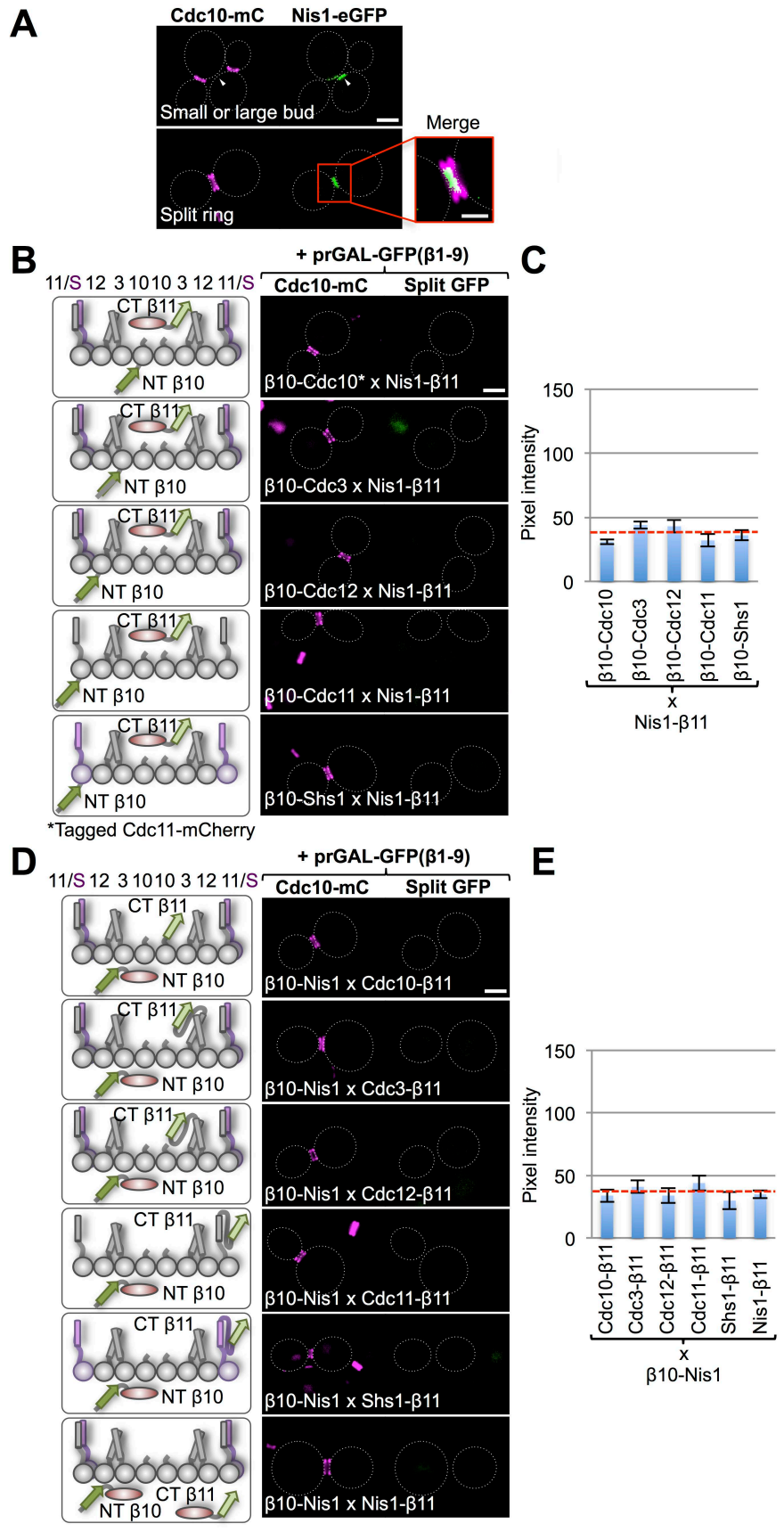
A
Cdc10-mC
Nis1-eGFP
Small or large bud
Merge
Split ring
B
+ prGAL-GFP(β1-9)
11/S 12 3 10 10 3 12 11/S
Cdc10-mC
Split GFP
CT β11
NT β10
β10-Cdc10* x Nis1-β11
β10-Cdc3 x Nis1-β11
β10-Cdc12 x Nis1-β11
β10-Cdc11 x Nis1-β11
β10-Shs1 x Nis1-β11
*Tagged Cdc11-mCherry
C
Pixel intensity
150
100
50
0
β10-Cdc10
β10-Cdc3
β10-Cdc12
β10-Cdc11
β10-Shs1
x
Nis1-β11
D
+ prGAL-GFP(β1-9)
11/S 12 3 10 10 3 12 11/S
Cdc10-mC
Split GFP
CT β11
NT β10
β10-Nis1 x Cdc10-β11
β10-Nis1 x Cdc3-β11
β10-Nis1 x Cdc12-β11
β10-Nis1 x Cdc11-β11
β10-Nis1 x Shs1-β11
β10-Nis1 x Nis1-β11
E
Pixel intensity
150
100
50
0
Cdc10-β11
Cdc3-β11
Cdc12-β11
Cdc11-β11
Shs1-β11
Nis1-β11
x
β10-Nis1

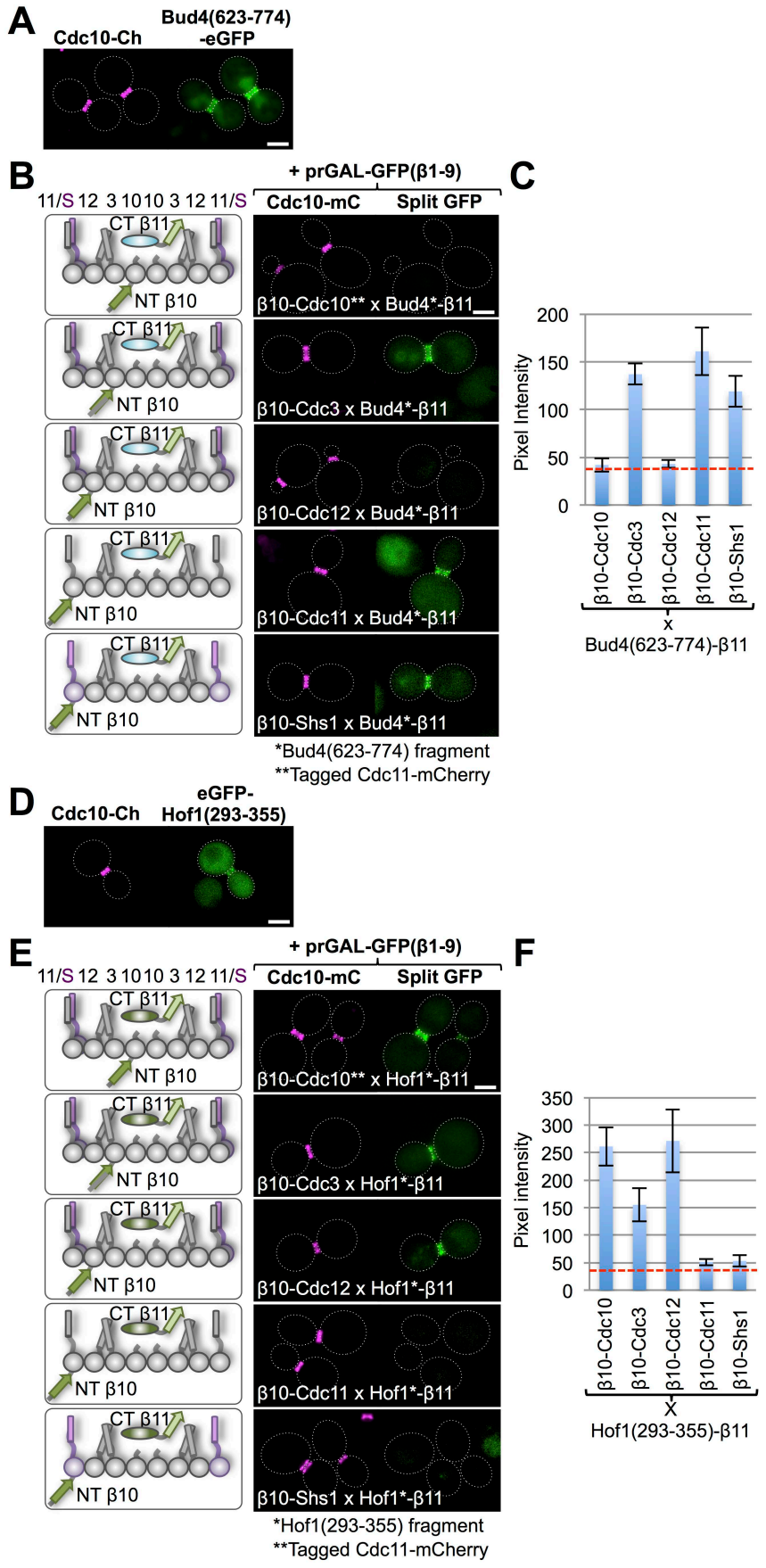
A
Cdc10-Ch
Bud4(623-774)
-eGFP
B
+ prGAL-GFP(β1-9)
11/S 12 3 10 10 3 12 11/S
Cdc10-mC
Split GFP
CT β11
NT β10
β10-Cdc10** x Bud4*-β11
β10-Cdc3 x Bud4*-β11
β10-Cdc12 x Bud4*-β11
β10-Cdc11 x Bud4*-β11
β10-Shs1 x Bud4*-β11
*Bud4(623-774) fragment
**Tagged Cdc11-mCherry
C
Pixel Intensity
200
150
100
50
0
β10-Cdc10
β10-Cdc3
β10-Cdc12
β10-Cdc11
β10-Shs1
x
Bud4(623-774)-β11
D
Cdc10-Ch
eGFP-
Hof1(293-355)
E
+ prGAL-GFP(β1-9)
11/S 12 3 10 10 3 12 11/S
Cdc10-mC
Split GFP
CT β11
NT β10
β10-Cdc10** x Hof1*-β11
β10-Cdc3 x Hof1*-β11
β10-Cdc12 x Hof1*-β11
β10-Cdc11 x Hof1*-β11
β10-Shs1 x Hof1*-β11
*Hof1(293-355) fragment
**Tagged Cdc11-mCherry
F
Pixel intensity
350
300
250
200
150
100
50
0
β10-Cdc10
β10-Cdc3
β10-Cdc12
β10-Cdc11
β10-Shs1
x
Hof1(293-355)-β11

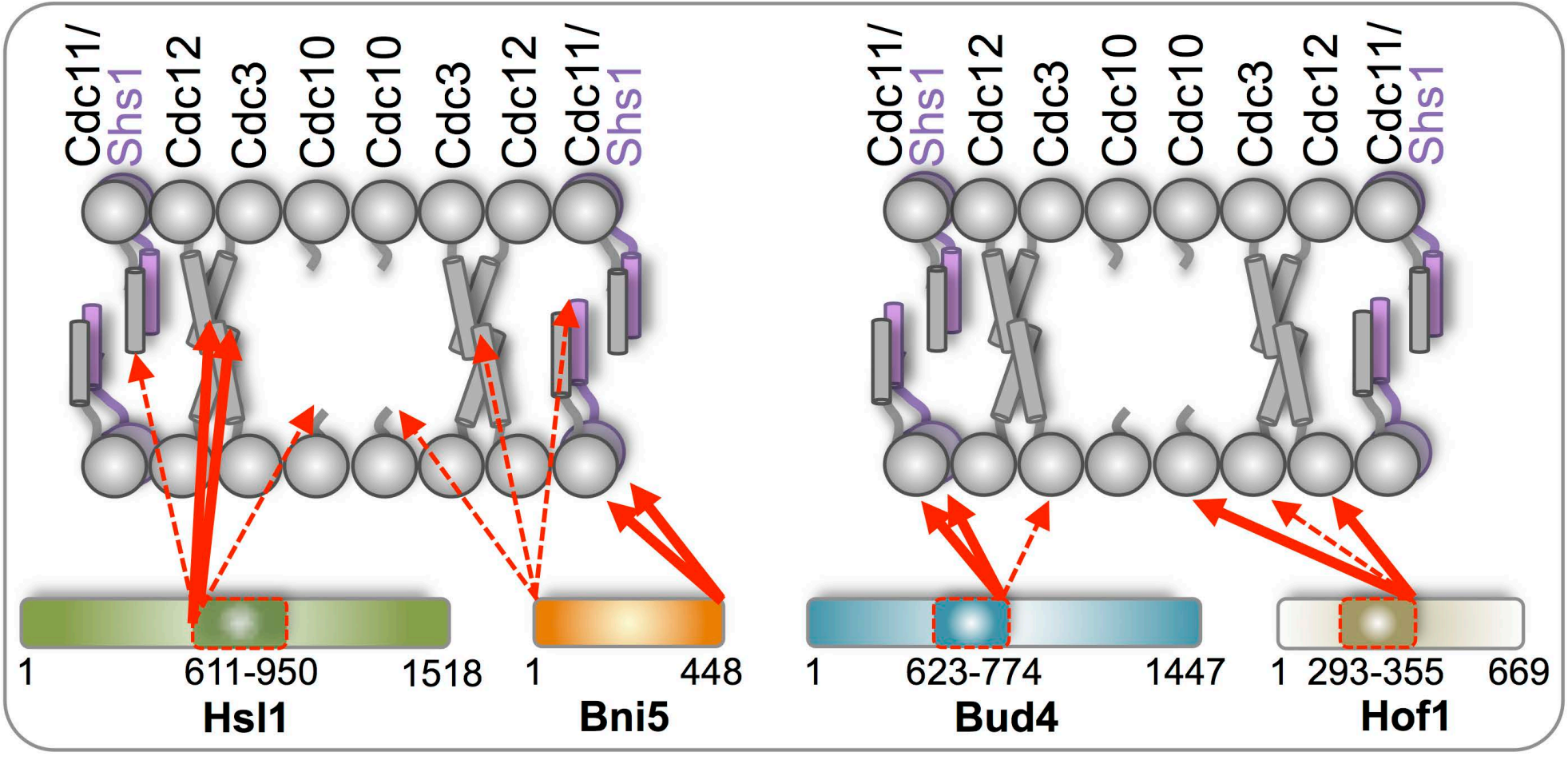
Cdc11/
Shs1
Cdc12
Cdc3
Cdc10
Cdc10
Cdc3
Cdc12
Cdc11/
Shs1
1
611-950
1518
1
448
Hsl1
Bni5
Cdc11/
Shs1
Cdc12
Cdc3
Cdc10
Cdc10
Cdc3
Cdc12
Cdc11/
Shs1
1
623-774
1447
1
293-355
669
Bud4
Hof1

SUPPORTING INFORMATION

for

Detection of protein-protein interactions at the septin collar in *Saccharomyces cerevisiae* using a tripartite split-GFP system

Gregory C. Finnigan,[†] Angela Duvalyan, Elizabeth N. Liao, Aspram Sargsyan

and Jeremy Thorner*

Division of Biochemistry, Biophysics and Structural Biology,

Department of Molecular and Cell Biology,

University of California, Berkeley, CA 94720-3202 USA

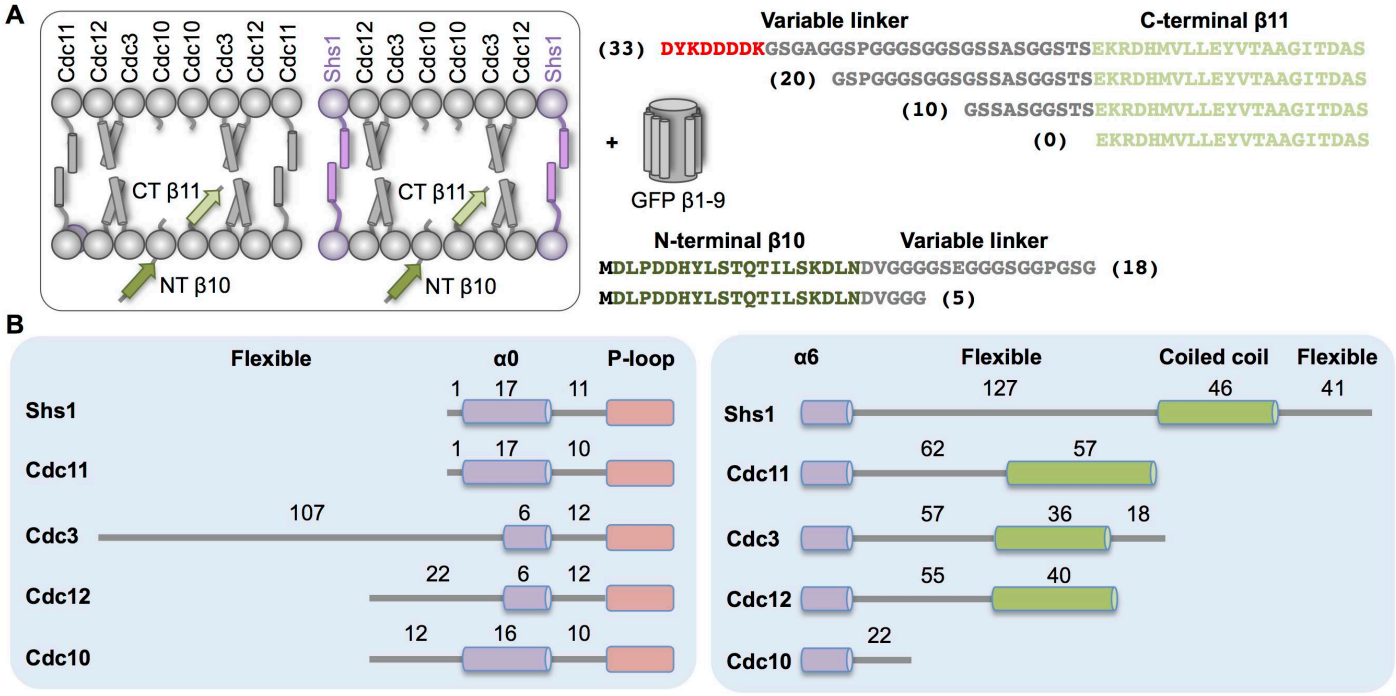

Figure S1. Tagging septin subunits for the tripartite split-GFP system. (A) *Left,* schematic diagram of the linear septin hetero-octamer, which can be capped with either of two alternative terminal subunits, Cdc11 or Shs1 (*purple*), and can polymerize end-to-end to form long laterally paired filaments. *Grey ball*, globular GTP-binding domain of each subunit; *cylinder,* C-terminal extension (CTE) with predicted α-helical and coiled coil-forming propensity (which only Cdc10 lacks); *dark green*, introduced N-terminal β10 tag; *light green*, introduced C-terminal β11 tag. When tagged versions of the same subunit are present in the diploid (*e.g.*, β10-Cdc10 and Cdc10-β11), no WT copy is present and 50% of the hetero-octamers will contain both tagged subunits. When two different tagged septins are combined (*e.g.*, β10-Cdc10 x Cdc3-β11), there is also a WT copy of each subunit present, which is not depicted in the diagram for clarity. In the latter case, in this representative subunit-subunit pairing (*e.g.*, β10-Cdc10 x Cdc3-β11), 7/16 (44%) of the hetero-octamers should contain both tagged subunits in a juxtaposed position. However, hetero-octamers are polymerized into filaments at the bud neck, greatly increasing the number of potential sites where juxtaposed tags will be present within any given septin collar, consequently the probability of detection (capture of the GFPβ1-9 barrel at multiple locations at the bud neck) is greatly enhanced. *Right,* C-terminal β11 tags were appended directly or with Ser- and Gly-rich linkers with the indicated lengths (10, 20 and 33 residues) and sequences indicated; N-terminal β10 tags were tethered, in most cases, by Gly-rich linkers of the lengths (5 and 18 residues) and sequences indicated. (B) Schematic representation of the naturally-occurring N-terminal (*left*) and C-terminal (*right*) extensions in the five yeast mitotic septins. Structure features follow the nomenclature of Sirajuddin *et al.* (2007).

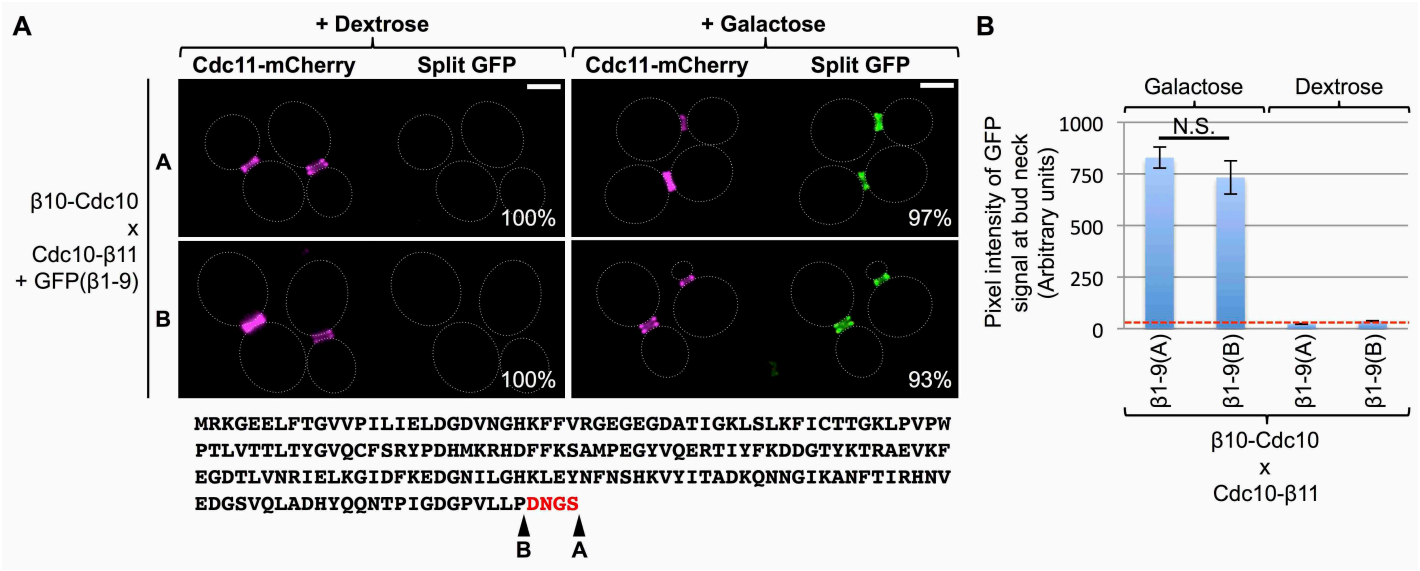

Figure S2. Both versions of the GFPβ1-9 barrel display robust GFP reconstitution *in vivo*. (A) In the initial report describing the tripartite split-GFP system (Cabantous et al., 2013), constructs of the GFPβ1-9 barrel that end at different positions after the 9th strand were used. Hence, we tested two such versions of GFPβ1-9 in yeast *in vivo*: A, which includes four additional residues (DNGS; *red*); and, B, ending after VLLP. Diploids (1 and 9, respectively) expressing β10-(linker)$_{32}$-Cdc10 and Cdc10-(linker)$_{33}$-β11, as well as Cdc11-mCherry, and carrying plasmids expressing either GFPβ1-9(A) (pGF-IVL794) or GFPβ1-9(B) (pGF-IVL795) from the inducible *GAL1/GAL10* promoter, were cultured overnight in 2% raffinose-0.2% sucrose medium selective for the presence of the plasmid, then back diluted into either the same medium containing 2% glucose (*left*) or 2% galactose (*right*), grown for 4.5 h, washed, and imaged by fluorescence microscopy. Glucose repression of either GFPβ1-9(A) or GFPβ1-9(B) expression prevented reconstitution of any GFP signal, whereas galactose induction of either GFPβ1-9(A) or GFPβ1-9(B) yielded equivalent, robust GFP fluorescence congruent with the bud neck marked with Cdc11-mCh. The percentage of the population (out of 50-100 representative budded cells) displaying the fluorescence pattern shown is indicated by the number in the lower right-hand corner of each panel. *Dotted white dotted line*, cell periphery; scale bar, 2 μm. (B) Quantification of the average pixel intensity of the GFP signal at the bud neck for the cultures shown in (A). *Dotted red line*, the average intrinsic background fluorescence of the bud neck in yeast cells lacking the components of the tripartite split-GFP system; *error bar*, S.E.M. There was no statistically significant difference (unpaired t-test, p = 0.325) between the average pixel intensity of the GFP signal at the bud neck when using either GFPβ1-9(A) or GFPβ1-9(B).

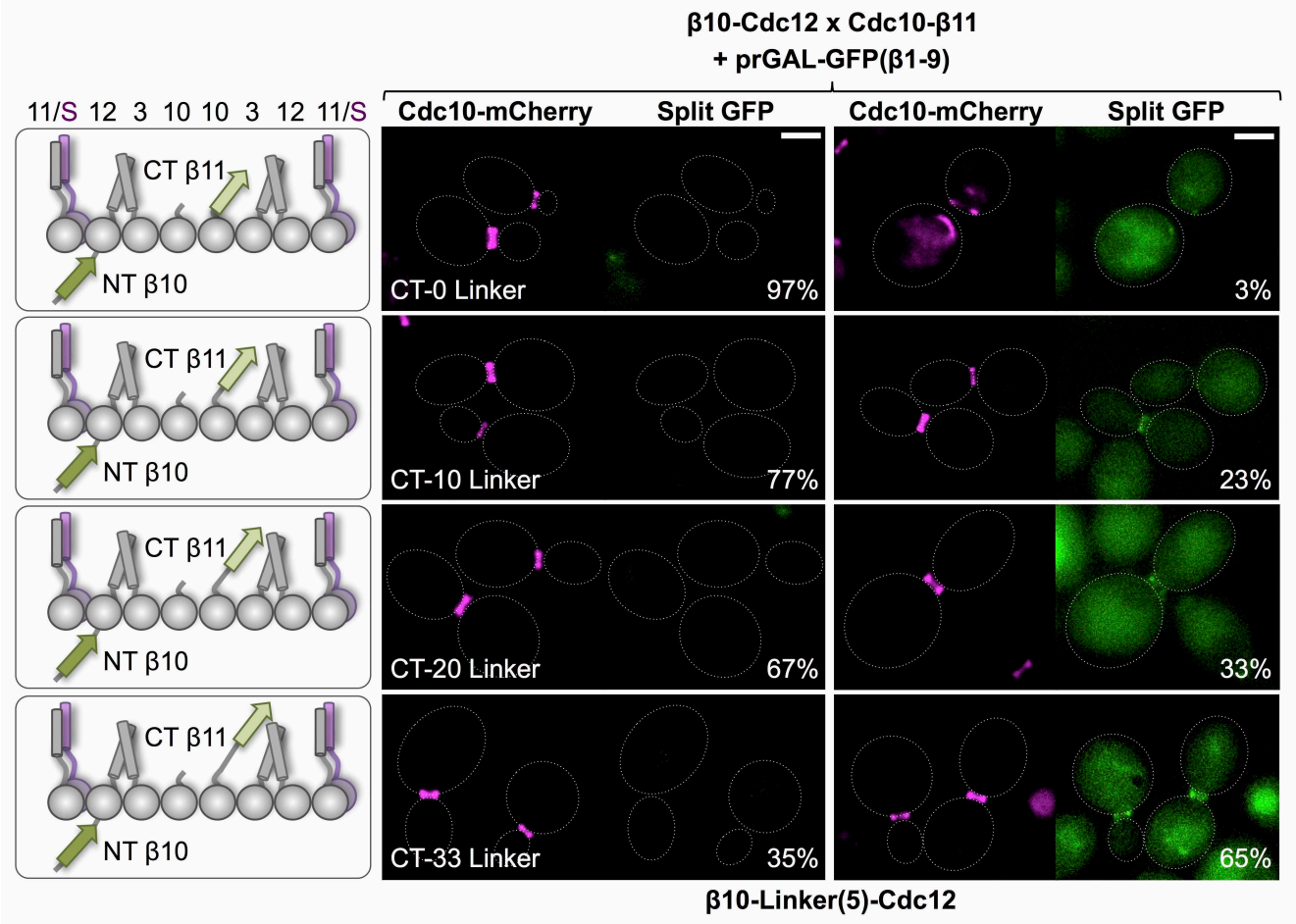

Figure S3. Interaction between Cdc10 and Cdc12 can be detected using the tripartite split-GFP method by extending the length of the linkers that tether the β10 and β11 tags. *Left*, schematic diagram of the septin hetero-octamer with the relative placement of the β10 and β11 tags on Cdc10 and Cdc12 (not precisely to scale). *Right*, Diploids (27, 13, 20, and 34) expressing β10-$(linker)_5$-Cdc12 (constant) with, respectively, Cdc10-β11, Cdc10-$(linker)_{10}$-β11, Cdc10-$(linker)_{20}$-β11, or Cdc10-$(linker)_{33}$-β11, as indicated, as well as Cdc10-mCh and a *CEN* plasmid expressing the GFPβ1-9 barrel from the *GAL1/GAL10* promoter (pGF-IVL794), were cultured, induce with galactose, harvested, washed and imaged by fluorescence microscopy as in Fig. S2A. The percentage of the population (out of 50-100 representative budded cells) displaying the fluorescence pattern shown is indicated by the number in the lower right-hand corner of each panel.

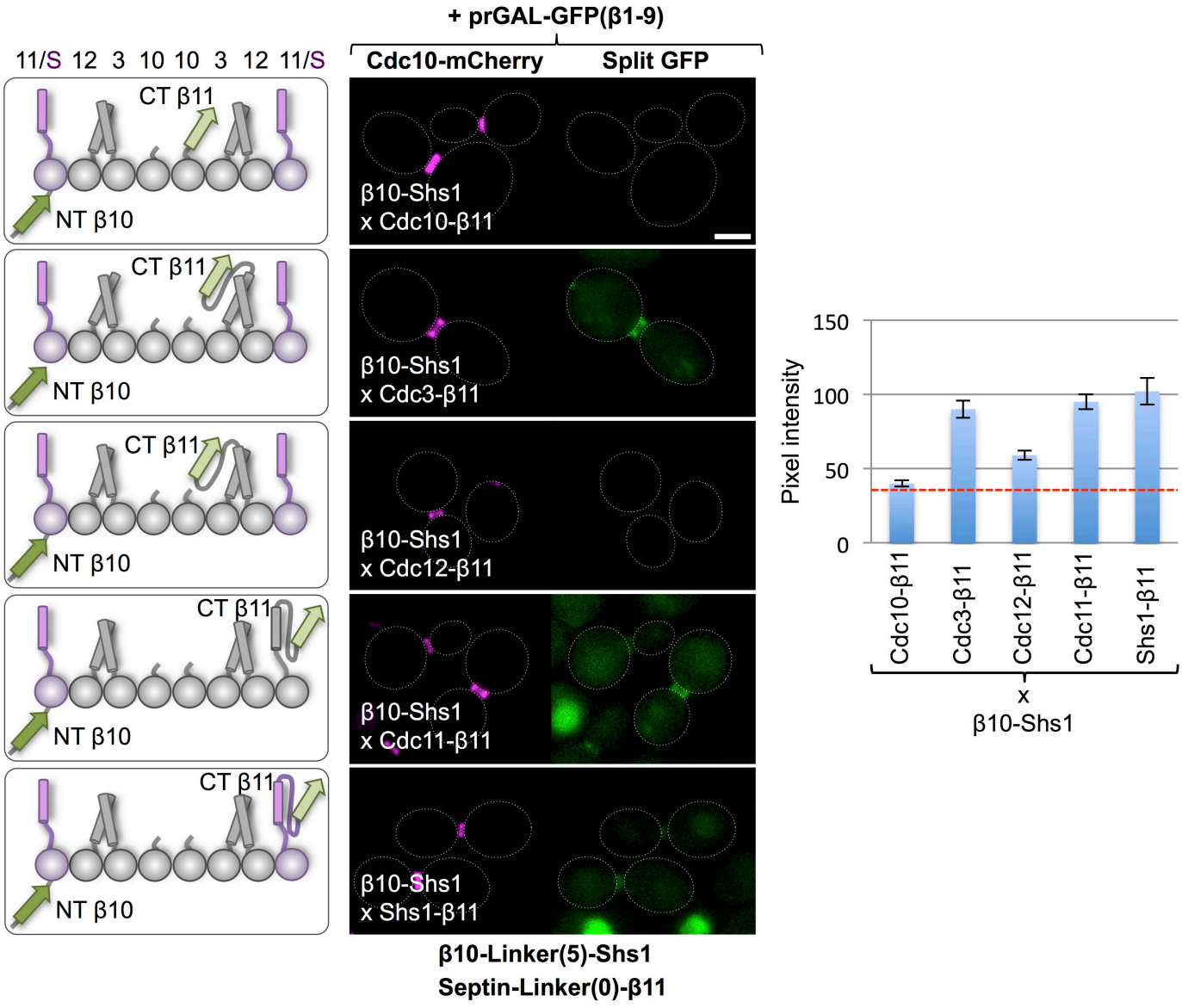

Figure S4. Interaction of the non-essential subunit Shs1 with the other mitotic septins assessed using the tripartite split-GFP method. (A) Diploids (108-112) expressing β10-(linker)$_5$-Shs1 and versions of all five mitotic septins to which the C-terminal β11 tag had been directly appended (i.e., no linker), and Cdc10-mCh (*left*), as well as the GFPβ1-9 barrel under the contorl of the *GAL1/GAL10* promoter on a *CEN* plasmid (pGF-IVL794) (*not shown*), were cultured, induced, harvested, washed and imaged by fluorescence microscopy as in Fig. S2A (*middle*). As always, the same exposure time was used for image capture and the images were scaled identically. *Dotted white lines*, cell periphery; scale bar, 2 μm. *Right, q*uantification using Image J of the average pixel intensity of the GFP signal at the bud neck (25-50 budded cells) for the cultures shown (*middle*). *Dotted red line*, the average intrinsic background fluorescence of the bud neck in yeast cells lacking the components of the tripartite split-GFP system; *error bar*, S.E.M

Table S1. Yeast strains used in Supplemental Figures 1-4.

Strain	**Genotype**	**Reference**
BY4741	*MAT**a** leu2Δ ura3Δ met15Δ his3Δ*	(Brachmann et al., 1998)
BY4742	*MAT**α** leu2Δ ura3Δ met15Δ his3Δ*	(Brachmann et al., 1998)
GFY-1794	BY4742; *cdc10Δ::GFPβ10::Linker(32)::CDC10::ADH1(t)::Hyg^R cdc11Δ::CDC11::mCherry::SpHIS5*	This study
GFY-1570	BY4741; *cdc10Δ::CDC10::Linker(33)::GFPβ11::ADH1(t)::Nat^R*	This study
GFY-1803	BY4742; *cdc12Δ::GFPβ10::Linker(5)::CDC12::ADH1(t)::Hyg^R cdc10Δ::CDC10::mCherry::SpHIS5*	This study
GFY-1851	BY4741; *cdc10Δ::CDC10::GFPβ11::ADH1(t)::Hyg^R*	This study
GFY-1852	BY4741; *cdc10Δ::CDC10::Linker(10)::GFPβ11::ADH1(t)::Hyg^R*	This study
GFY-1853	BY4741; *cdc10Δ::CDC10::Linker(20)::GFPβ11::ADH1(t)::Hyg^R*	This study
GFY-1807	BY4742; *shs1Δ::GFPβ10::Linker(5)::SHS1::ADH1(t)::Hyg^R cdc10Δ::CDC10::mCherry::SpHIS5*	This study
GFY-1845	BY4741; *cdc3Δ::CDC3::GFPβ11::ADH1(t)::Hyg^R*	This study
GFY-1848	BY4741; *cdc12Δ::CDC12::GFPβ11::ADH1(t)::Hyg^R*	This study
GFY-1842	BY4741; *cdc11Δ::CDC11::GFPβ11::ADH1(t)::Hyg^R*	This study
GFY-1839	BY4741; *shs1Δ::SHS1::GFPβ11::ADH1(t)::Hyg^R*	This study

Table S2. Plasmids used in Supplemental Figures 1-4.

pRS315	CEN; *LEU2 AMP*	(Sikorski and Hieter, 1989)
pGF-IVL794	pRS315; *prGAL1/10::GFPβ1-9(A)::ADH1(t)::Kan^R*	This study
pGF-IVL795	pRS315; *prGAL1/10::GFPβ1-9(B)::ADH1(t)::Kan^R*	This study

Table S3. Diploid strains used in this study.

Diploid Number	**Haploid strains crossed (+ plamids)**	**Notes[2]**
1[1]	GFY-1794 x GFY-1570 (+pGF-IVL794)	Negative Controls
2	GFY-1794 x BY4741 (+pGF-IVL794)	Negative Controls
3	GFY-59 x GFY-1570 (+pGF-IVL794)	Negative Controls
4	GFY-59 x BY4741 (+pGF-IVL794)	Negative Controls
5	GFY-59 x BY4741 (+pRS315 empty)	Negative Controls
6	GFY-1794 x GFY-1570 (+pRS315 empty)	Negative Controls
7	GFY-59 x GFY-1570 (+pRS315 empty)	Negative Controls
8	GFY-1794 x BY4741 (+pRS315 empty)	Negative Controls
9	GFY-1794 x GFY-1570 (+pGF-IVL795)	Negative Controls
164	GFY-1793 x GFY-1979 (+pGF-IVL794)	Neg. Controls (Pgk1)
165	GFY-1796 x GFY-1979 (+pGF-IVL794)	Neg. Controls (Pgk1)
166	GFY-1795 x GFY-1979 (+pGF-IVL794)	Neg. Controls (Pgk1)
167	GFY-1797 x GFY-1979 (+pGF-IVL794)	Neg. Controls (Pgk1)
168	GFY-1806 x GFY-1979 (+pGF-IVL794)	Neg. Controls (Pgk1)
170	GFY-1793 x GFY-1983 (+pGF-IVL794)	Neg. Controls (Hsp82)
171	GFY-1796 x GFY-1983 (+pGF-IVL794)	Neg. Controls (Hsp82)
172	GFY-1795 x GFY-1983 (+pGF-IVL794)	Neg. Controls (Hsp82)
173	GFY-1797 x GFY-1983 (+pGF-IVL794)	Neg. Controls (Hsp82)
174	GFY-1806 x GFY-1983 (+pGF-IVL794)	Neg. Controls (Hsp82)

272	GFY-1793 x GFY-2035 (+pGF-IVL794)	Neg. Controls (Cdc19)
273	GFY-1796 x GFY-2035 (+pGF-IVL794)	Neg. Controls (Cdc19)
274	GFY-1795 x GFY-2035 (+pGF-IVL794)	Neg. Controls (Cdc19)
275	GFY-1797 x GFY-2035 (+pGF-IVL794)	Neg. Controls (Cdc19)
276	GFY-1806 x GFY-2035 (+pGF-IVL794)	Neg. Controls (Cdc19)
277	GFY-1793 x GFY-2036 (+pGF-IVL794)	Neg. Controls (Gpp1)
278	GFY-1796 x GFY-2036 (+pGF-IVL794)	Neg. Controls (Gpp1)
279	GFY-1795 x GFY-2036 (+pGF-IVL794)	Neg. Controls (Gpp1)
280	GFY-1797 x GFY-2036 (+pGF-IVL794)	Neg. Controls (Gpp1)
281	GFY-1806 x GFY-2036 (+pGF-IVL794)	Neg. Controls (Gpp1)
282	GFY-1793 x GFY-2043 (+pGF-IVL794)	Neg. Controls (Tpi1)
283	GFY-1796 x GFY-2043 (+pGF-IVL794)	Neg. Controls (Tpi1)
284	GFY-1795 x GFY-2043 (+pGF-IVL794)	Neg. Controls (Tpi1)
285	GFY-1797 x GFY-2043 (+pGF-IVL794)	Neg. Controls (Tpi1)
286	GFY-1806 x GFY-2043 (+pGF-IVL794)	Neg. Controls (Tpi1)
25	GFY-1801 x GFY-1851 (+pGF-IVL794)	Septin x Septin (Cdc10-β11)
24	GFY-1798 x GFY-1851 (+pGF-IVL794)	Septin x Septin (Cdc10-β11)
27	GFY-1803 x GFY-1851 (+pGF-IVL794)	Septin x Septin (Cdc10-β11)
26	GFY-1804 x GFY-1851 (+pGF-IVL794)	Septin x Septin (Cdc10-β11)
28	GFY-1807 x GFY-1851 (+pGF-IVL794)	Septin x Septin (Cdc10-β11)
39	GFY-1796 x GFY-1851 (+pGF-IVL794)	Septin x Septin (Cdc10-β11)

38	GFY-1793 x GFY-1851 (+pGF-IVL794)	Septin x Septin (Cdc10-β11)
41	GFY-1797 x GFY-1851 (+pGF-IVL794)	Septin x Septin (Cdc10-β11)
40	GFY-1795 x GFY-1851 (+pGF-IVL794)	Septin x Septin (Cdc10-β11)
42	GFY-1806 x GFY-1851 (+pGF-IVL794)	Septin x Septin (Cdc10-β11)
11	GFY-1801 x GFY-1852 (+pGF-IVL794)	Septin x Septin (Cdc10-β11)
10	GFY-1798 x GFY-1852 (+pGF-IVL794)	Septin x Septin (Cdc10-β11)
13	GFY-1803 x GFY-1852 (+pGF-IVL794)	Septin x Septin (Cdc10-β11)
12	GFY-1804 x GFY-1852 (+pGF-IVL794)	Septin x Septin (Cdc10-β11)
14	GFY-1807 x GFY-1852 (+pGF-IVL794)	Septin x Septin (Cdc10-β11)
46	GFY-1796 x GFY-1852 (+pGF-IVL794)	Septin x Septin (Cdc10-β11)
45	GFY-1793 x GFY-1852 (+pGF-IVL794)	Septin x Septin (Cdc10-β11)
48	GFY-1797 x GFY-1852 (+pGF-IVL794)	Septin x Septin (Cdc10-β11)
47	GFY-1795 x GFY-1852 (+pGF-IVL794)	Septin x Septin (Cdc10-β11)
49	GFY-1806 x GFY-1852 (+pGF-IVL794)	Septin x Septin (Cdc10-β11)
18	GFY-1801 x GFY-1853 (+pGF-IVL794)	Septin x Septin (Cdc10-β11)
17	GFY-1798 x GFY-1853 (+pGF-IVL794)	Septin x Septin (Cdc10-β11)
20	GFY-1803 x GFY-1853 (+pGF-IVL794)	Septin x Septin (Cdc10-β11)
19	GFY-1804 x GFY-1853 (+pGF-IVL794)	Septin x Septin (Cdc10-β11)
21	GFY-1807 x GFY-1853 (+pGF-IVL794)	Septin x Septin (Cdc10-β11)
53	GFY-1796 x GFY-1853 (+pGF-IVL794)	Septin x Septin (Cdc10-β11)
52	GFY-1793 x GFY-1853 (+pGF-IVL794)	Septin x Septin (Cdc10-β11)

55	GFY-1797 x GFY-1853 (+pGF-IVL794)	Septin x Septin (Cdc10-β11)
54	GFY-1795 x GFY-1853 (+pGF-IVL794)	Septin x Septin (Cdc10-β11)
56	GFY-1806 x GFY-1853 (+pGF-IVL794)	Septin x Septin (Cdc10-β11)
32	GFY-1801 x GFY-1570 (+pGF-IVL794)	Septin x Septin (Cdc10-β11)
31	GFY-1798 x GFY-1570 (+pGF-IVL794)	Septin x Septin (Cdc10-β11)
34	GFY-1803 x GFY-1570 (+pGF-IVL794)	Septin x Septin (Cdc10-β11)
33	GFY-1804 x GFY-1570 (+pGF-IVL794)	Septin x Septin (Cdc10-β11)
35	GFY-1807 x GFY-1570 (+pGF-IVL794)	Septin x Septin (Cdc10-β11)
60	GFY-1796 x GFY-1570 (+pGF-IVL794)	Septin x Septin (Cdc10-β11)
59	GFY-1793 x GFY-1570 (+pGF-IVL794)	Septin x Septin (Cdc10-β11)
62	GFY-1797 x GFY-1570 (+pGF-IVL794)	Septin x Septin (Cdc10-β11)
61	GFY-1795 x GFY-1570 (+pGF-IVL794)	Septin x Septin (Cdc10-β11)
63	GFY-1806 x GFY-1570 (+pGF-IVL794)	Septin x Septin (Cdc10-β11)
67	GFY-1798 x GFY-1851 (+pGF-IVL794)	Septin x Septin (β10-Cdc3)
66	GFY-1798 x GFY-1845 (+pGF-IVL794)	Septin x Septin (β10-Cdc3)
69	GFY-1798 x GFY-1848 (+pGF-IVL794)	Septin x Septin (β10-Cdc3)
68	GFY-1798 x GFY-1842 (+pGF-IVL794)	Septin x Septin (β10-Cdc3)
70	GFY-1798 x GFY-1839 (+pGF-IVL794)	Septin x Septin (β10-Cdc3)
74	GFY-1801 x GFY-1851 (+pGF-IVL794)	Septin x Septin (β10-Cdc10)
73	GFY-1801 x GFY-1845 (+pGF-IVL794)	Septin x Septin (β10-Cdc10)
76	GFY-1801 x GFY-1848 (+pGF-IVL794)	Septin x Septin (β10-Cdc10)

75	GFY-1801 x GFY-1842 (+pGF-IVL794)	Septin x Septin (β10-Cdc10)
77	GFY-1801 x GFY-1839 (+pGF-IVL794)	Septin x Septin (β10-Cdc10)
81	GFY-1804 x GFY-1851 (+pGF-IVL794)	Septin x Septin (β10-Cdc11)
80	GFY-1804 x GFY-1845 (+pGF-IVL794)	Septin x Septin (β10-Cdc11)
83	GFY-1804 x GFY-1848 (+pGF-IVL794)	Septin x Septin (β10-Cdc11)
82	GFY-1804 x GFY-1842 (+pGF-IVL794)	Septin x Septin (β10-Cdc11)
84	GFY-1804 x GFY-1839 (+pGF-IVL794)	Septin x Septin (β10-Cdc11)
109	GFY-1807 x GFY-1851 (+pGF-IVL794)	Septin x Septin (β10-Shs1)
108	GFY-1807 x GFY-1845 (+pGF-IVL794)	Septin x Septin (β10-Shs1)
111	GFY-1807 x GFY-1848 (+pGF-IVL794)	Septin x Septin (β10-Shs1)
110	GFY-1807 x GFY-1842 (+pGF-IVL794)	Septin x Septin (β10-Shs1)
112	GFY-1807 x GFY-1839 (+pGF-IVL794)	Septin x Septin (β10-Shs1)
102	GFY-1803 x GFY-1851 (+pGF-IVL794)	Septin x Septin (β10-Cdc12)
101	GFY-1803 x GFY-1845 (+pGF-IVL794)	Septin x Septin (β10-Cdc12)
104	GFY-1803 x GFY-1848 (+pGF-IVL794)	Septin x Septin (β10-Cdc12)
103	GFY-1803 x GFY-1842 (+pGF-IVL794)	Septin x Septin (β10-Cdc12)
105	GFY-1803 x GFY-1839 (+pGF-IVL794)	Septin x Septin (β10-Cdc12)
151	GFY-1809 x GFY-1570 (+pGF-IVL794)	Septin x β10-Bni5
150	GFY-1809 x GFY-1572 (+pGF-IVL794)	Septin x β10-Bni5
153	GFY-1809 x GFY-1571 (+pGF-IVL794)	Septin x β10-Bni5
152	GFY-1809 x GFY-1573 (+pGF-IVL794)	Septin x β10-Bni5

154	GFY-1809 x GFY-1567 (+pGF-IVL794)	Septin x β10-Bni5
155	GFY-1809 x GFY-1735 (+pGF-IVL794)	Bni5-β11 x β10-Bni5
127	GFY-1796 x GFY-1735 (+pGF-IVL794)	Septin x Bni5-β11
120	GFY-1793 x GFY-1735 (+pGF-IVL794)	Septin x Bni5-β11
141	GFY-1797 x GFY-1735 (+pGF-IVL794)	Septin x Bni5-β11
134	GFY-1795 x GFY-1735 (+pGF-IVL794)	Septin x Bni5-β11
148	GFY-1806 x GFY-1735 (+pGF-IVL794)	Septin x Bni5-β11
158	GFY-1899 x GFY-1570 (+pGF-IVL794)	Septin x β10-Nis1
157	GFY-1899 x GFY-1572 (+pGF-IVL794)	Septin x β10-Nis1
160	GFY-1899 x GFY-1571 (+pGF-IVL794)	Septin x β10-Nis1
159	GFY-1899 x GFY-1573 (+pGF-IVL794)	Septin x β10-Nis1
161	GFY-1899 x GFY-1567 (+pGF-IVL794)	Septin x β10-Nis1
163	GFY-1899 x GFY-1854 (+pGF-IVL794)	Nis1-β11 x β10-Nis1
128	GFY-1796 x GFY-1854 (+pGF-IVL794)	Septin x Nis1-β11
121	GFY-1793 x GFY-1854 (+pGF-IVL794)	Septin x Nis1-β11
142	GFY-1797 x GFY-1854 (+pGF-IVL794)	Septin x Nis1-β11
135	GFY-1795 x GFY-1854 (+pGF-IVL794)	Septin x Nis1-β11
149	GFY-1806 x GFY-1854 (+pGF-IVL794)	Septin x Nis1-β11
177	GFY-1992 x GFY-1570 (+pGF-IVL794)	Septin x Hsl1(WT)
176	GFY-1992 x GFY-1572 (+pGF-IVL794)	Septin x Hsl1(WT)
179	GFY-1992 x GFY-1571 (+pGF-IVL794)	Septin x Hsl1(WT)

178	GFY-1992 x GFY-1573 (+pGF-IVL794)	Septin x Hsl1(WT)
180	GFY-1992 x GFY-1567 (+pGF-IVL794)	Septin x Hsl1(WT)
182	GFY-1995 x GFY-1570 (+pGF-IVL794)	Septin x Hsl1(611-950)
181	GFY-1995 x GFY-1572 (+pGF-IVL794)	Septin x Hsl1(611-950)
184	GFY-1995 x GFY-1571 (+pGF-IVL794)	Septin x Hsl1(611-950)
183	GFY-1995 x GFY-1573 (+pGF-IVL794)	Septin x Hsl1(611-950)
185	GFY-1995 x GFY-1567 (+pGF-IVL794)	Septin x Hsl1(611-950)
187	GFY-1997 x GFY-1570 (+pGF-IVL794)	Septin x Hsl1(611-950; 1245-1518)
186	GFY-1997 x GFY-1572 (+pGF-IVL794)	Septin x Hsl1(611-950; 1245-1518)
189	GFY-1997 x GFY-1571 (+pGF-IVL794)	Septin x Hsl1(611-950; 1245-1518)
188	GFY-1997 x GFY-1573 (+pGF-IVL794)	Septin x Hsl1(611-950; 1245-1518)
190	GFY-1997 x GFY-1567 (+pGF-IVL794)	Septin x Hsl1(611-950; 1245-1518)
216	GFY-1997 x GFY-1846 (+pGF-IVL794)	Septin x Hsl1(611-950; 1245-1518)
217	GFY-1997 x GFY-1852 (+pGF-IVL794)	Septin x Hsl1(611-950; 1245-1518)
218	GFY-1997 x GFY-1843 (+pGF-IVL794)	Septin x Hsl1(611-950; 1245-1518)
219	GFY-1997 x GFY-1849 (+pGF-IVL794)	Septin x Hsl1(611-950; 1245-1518)
220	GFY-1997 x GFY-1840 (+pGF-IVL794)	Septin x Hsl1(611-950; 1245-1518)
221	GFY-1997 x GFY-1847 (+pGF-IVL794)	Septin x Hsl1(611-950; 1245-1518)
222	GFY-1997 x GFY-1853 (+pGF-IVL794)	Septin x Hsl1(611-950; 1245-1518)
223	GFY-1997 x GFY-1844 (+pGF-IVL794)	Septin x Hsl1(611-950; 1245-1518)
224	GFY-1997 x GFY-2044 (+pGF-IVL794)	Septin x Hsl1(611-950; 1245-1518)

225	GFY-1997 x GFY-1841 (+pGF-IVL794)	Septin x Hsl1(611-950; 1245-1518)
262	GFY-1997 x GFY-1845 (+pGF-IVL794)	Septin x Hsl1(611-950; 1245-1518)
263	GFY-1997 x GFY-1851 (+pGF-IVL794)	Septin x Hsl1(611-950; 1245-1518)
264	GFY-1997 x GFY-1842 (+pGF-IVL794)	Septin x Hsl1(611-950; 1245-1518)
265	GFY-1997 x GFY-1848 (+pGF-IVL794)	Septin x Hsl1(611-950; 1245-1518)
266	GFY-1997 x GFY-1839 (+pGF-IVL794)	Septin x Hsl1(611-950; 1245-1518)
206	GFY-1996 x GFY-1846 (+pGF-IVL794)	Septin x Hsl1(611-950; 1245-1518)
207	GFY-1996 x GFY-1852 (+pGF-IVL794)	Septin x Hsl1(611-950; 1245-1518)
208	GFY-1996 x GFY-1843 (+pGF-IVL794)	Septin x Hsl1(611-950; 1245-1518)
209	GFY-1996 x GFY-1849 (+pGF-IVL794)	Septin x Hsl1(611-950; 1245-1518)
210	GFY-1996 x GFY-1840 (+pGF-IVL794)	Septin x Hsl1(611-950; 1245-1518)
211	GFY-1996 x GFY-1847 (+pGF-IVL794)	Septin x Hsl1(611-950; 1245-1518)
212	GFY-1996 x GFY-1853 (+pGF-IVL794)	Septin x Hsl1(611-950; 1245-1518)
213	GFY-1996 x GFY-1844 (+pGF-IVL794)	Septin x Hsl1(611-950; 1245-1518)
214	GFY-1996 x GFY-2044 (+pGF-IVL794)	Septin x Hsl1(611-950; 1245-1518)
215	GFY-1996 x GFY-1841 (+pGF-IVL794)	Septin x Hsl1(611-950; 1245-1518)
252	GFY-1996 x GFY-1572 (+pGF-IVL794)	Septin x Hsl1(611-950; 1245-1518)
253	GFY-1996 x GFY-1570 (+pGF-IVL794)	Septin x Hsl1(611-950; 1245-1518)
254	GFY-1996 x GFY-1573 (+pGF-IVL794)	Septin x Hsl1(611-950; 1245-1518)
255	GFY-1996 x GFY-1571 (+pGF-IVL794)	Septin x Hsl1(611-950; 1245-1518)
256	GFY-1996 x GFY-1567 (+pGF-IVL794)	Septin x Hsl1(611-950; 1245-1518)

257	GFY-1996 x GFY-1845 (+pGF-IVL794)	Septin x Hsl1(611-950; 1245-1518)
258	GFY-1996 x GFY-1851 (+pGF-IVL794)	Septin x Hsl1(611-950; 1245-1518)
259	GFY-1996 x GFY-1842 (+pGF-IVL794)	Septin x Hsl1(611-950; 1245-1518)
260	GFY-1996 x GFY-1848 (+pGF-IVL794)	Septin x Hsl1(611-950; 1245-1518)
261	GFY-1996 x GFY-1839 (+pGF-IVL794)	Septin x Hsl1(611-950; 1245-1518)
226	GFY-1998 x GFY-1846 (+pGF-IVL794)	Septin x Hsl1(611-950; 1245-1518)
227	GFY-1998 x GFY-1852 (+pGF-IVL794)	Septin x Hsl1(611-950; 1245-1518)
228	GFY-1998 x GFY-1843 (+pGF-IVL794)	Septin x Hsl1(611-950; 1245-1518)
229	GFY-1998 x GFY-1849 (+pGF-IVL794)	Septin x Hsl1(611-950; 1245-1518)
230	GFY-1998 x GFY-1840 (+pGF-IVL794)	Septin x Hsl1(611-950; 1245-1518)
231	GFY-1998 x GFY-1847 (+pGF-IVL794)	Septin x Hsl1(611-950; 1245-1518)
232	GFY-1998 x GFY-1853 (+pGF-IVL794)	Septin x Hsl1(611-950; 1245-1518)
233	GFY-1998 x GFY-1844 (+pGF-IVL794)	Septin x Hsl1(611-950; 1245-1518)
234	GFY-1998 x GFY-2044 (+pGF-IVL794)	Septin x Hsl1(611-950; 1245-1518)
235	GFY-1998 x GFY-1841 (+pGF-IVL794)	Septin x Hsl1(611-950; 1245-1518)
247	GFY-1998 x GFY-1845 (+pGF-IVL794)	Septin x Hsl1(611-950; 1245-1518)
248	GFY-1998 x GFY-1851 (+pGF-IVL794)	Septin x Hsl1(611-950; 1245-1518)
249	GFY-1998 x GFY-1842 (+pGF-IVL794)	Septin x Hsl1(611-950; 1245-1518)
250	GFY-1998 x GFY-1848 (+pGF-IVL794)	Septin x Hsl1(611-950; 1245-1518)
251	GFY-1998 x GFY-1839 (+pGF-IVL794)	Septin x Hsl1(611-950; 1245-1518)

267	GFY-1998 x GFY-1572 (+pGF-IVL794)	Septin x Hsl1(611-950; 1245-1518)
268	GFY-1998 x GFY-1570 (+pGF-IVL794)	Septin x Hsl1(611-950; 1245-1518)
269	GFY-1998 x GFY-1573 (+pGF-IVL794)	Septin x Hsl1(611-950; 1245-1518)
270	GFY-1998 x GFY-1571 (+pGF-IVL794)	Septin x Hsl1(611-950; 1245-1518)
271	GFY-1998 x GFY-1567 (+pGF-IVL794)	Septin x Hsl1(611-950; 1245-1518)
287[3]	GFY-1796 (+pGF-IVL1084) x BY4741 (+pGF-IVL1005)	Septins x Bud4(623-774)
288	GFY-1793 (+pGF-IVL1084) x BY4741 (+pGF-IVL1005)	Septins x Bud4(623-774)
289	GFY-1795 (+pGF-IVL1084) x BY4741 (+pGF-IVL1005)	Septins x Bud4(623-774)
290	GFY-1797 (+pGF-IVL1084) x BY4741 (+pGF-IVL1005)	Septins x Bud4(623-774)
291	GFY-1806 (+pGF-IVL1084) x BY4741 (+pGF-IVL1005)	Septins x Bud4(623-774)
292	GFY-1796 (+pGF-IVL1082) x BY4741 (+pGF-IVL1005)	Septins x Hof1(293-355)
293	GFY-1793 (+pGF-IVL1082) x BY4741 (+pGF-IVL1005)	Septins x Hof1(293-355)
294	GFY-1795 (+pGF-IVL1082) x BY4741 (+pGF-IVL1005)	Septins x Hof1(293-355)
295	GFY-1797 (+pGF-IVL1082) x BY4741 (+pGF-IVL1005)	Septins x Hof1(293-355)

296	GFY-1806 (+pGF-IVL1082) x BY4741 (+pGF-IVL1005)	Septins x Hof1(293-355)

[1]For all diploids, unless otherwise noted, the plasmid expressing GFPβ1-9 was transformed into the *MAT**a*** strain prior to mating and diploid selection. Additionally, all haploid strains were selected on medium containing 5-FOA to counter-select for any covering vectors expressing WT copies of the septin gene(s). Unless otherwise noted, yeast were mated on YPD for 24 hours at 30°C and replica-plated to SD-HIS-LEU, grown for 2 days, and transferred to a second SD-HIS-LEU plate and grown for 1-2 additional days.

[2]For clarity, the general category and description of each small grouping of diploid strains is given. In general, one protein fusion is held constant and compared against the remaining set of five tagged septins. The portion held constant in each grouping is briefly described (e.g. Cdc10-β11).

[3]Diploids strains expressing fragments of either Bud4 or Hof1 (expressed from plasmids) used a modified diploid selection procedure. Prior to transformation of the GFPβ1-9 plasmid or Bud4/Hof1-expressing plasmids, the septin covering vector was counter-selected on 5-FOA medium twice. Following mating, diploids were selected on SD-URA-LEU medium twice.

Table S4. Protein abundance for split GFP negative control proteins present in the cytosol

Protein	Description	Molecules / cell	Reference
Pgk1	3-phosphoglycerate kinase	314,000	(Ghaemmaghami et al., 2003)
		15,100	(Chong et al., 2015)
		561,265	(Kulak et al., 2014)
		42,840	(Newman et al., 2006)
Hsp82	Hsp90 protein chaperone	445,000	(Ghaemmaghami et al., 2003)
		4,167	(Chong et al., 2015)
		10,044	(Kulak et al., 2014)
		6,395	(Newman et al., 2006)
Gpp1	Glycerol-1-phosphatase	193,000	(Ghaemmaghami et al., 2003)
		14,626	(Chong et al., 2015)
		235,727	(Kulak et al., 2014)
		9,107	(Newman et al., 2006)
Tpi1	Triose phosphate isomerase	207,000	(Ghaemmaghami et al., 2003)
		5,770	(Chong et al., 2015)
		395,237	(Kulak et al., 2014)
		4,768	(Newman et al., 2006)
Cdc19	Pyruvate kinase	291,000	(Ghaemmaghami et al., 2003)
		404,162	(Kulak et al., 2014)
		11,387	(Newman et al., 2006)
Cdc11	Septin subunit	9280	(Ghaemmaghami et al., 2003)
		236	(Chong et al., 2015)
		3947	(Kulak et al., 2014)
		359	(Newman et al., 2006)

SUPPLEMENTAL LITERATURE CITED

Brachmann, C.B., Davies, A., Cost, G.J., Caputo, E., Li, J., Hieter, P., and Boeke, J.D. (1998). Designer deletion strains derived from *Saccharomyces cerevisiae* S288C: a useful set of strains and plasmids for PCR-mediated gene disruption and other applications. Yeast *14*, 115-132.

Cabantous, S., Nguyen, H.B., Pedelacq, J.D., Koraichi, F., Chaudhary, A., Ganguly, K., Lockard, M.A., Favre, G., Terwilliger, T.C., and Waldo, G.S. (2013). A new protein-protein interaction sensor based on tripartite split-GFP association. Sci Rep *3*, 2854.1-2854.9.

Chong, Y.T., Koh, J.L., Friesen, H., Duffy, S.K., Cox, M.J., Moses, A., Moffat, J., Boone, C., and Andrews, B.J. (2015). Yeast proteome dynamics from single cell imaging and automated analysis. Cell *161*, 1413-1424.

Ghaemmaghami, S., Huh, W.K., Bower, K., Howson, R.W., Belle, A., Dephoure, N., O'Shea, E.K., and Weissman, J.S. (2003). Global analysis of protein expression in yeast. Nature *425*, 737-741.

Kulak, N.A., Pichler, G., Paron, I., Nagaraj, N., and Mann, M. (2014). Minimal, encapsulated proteomic-sample processing applied to copy-number estimation in eukaryotic cells. Nat Methods *11*, 319-324.

Newman, J.R., Ghaemmaghami, S., Ihmels, J., Breslow, D.K., Noble, M., DeRisi, J.L., and Weissman, J.S. (2006). Single-cell proteomic analysis of *S. cerevisiae* reveals the architecture of biological noise. Nature *441*, 840-846.

Sikorski, R.S., and Hieter, P. (1989). A system of shuttle vectors and yeast host strains designed for efficient manipulation of DNA in *Saccharomyces cerevisiae*. Genetics *122*, 19-27.

Sirajuddin, M., Farkasovsky, M., Hauer, F., Kühlmann, D., Macara, I.G., Weyand., M. Stark, H., Wittinghofer, A. (2007) Structural insight into filament formation by mammalian septins. Nature *449*, 311-315.